Supporting Information

Gold(III) pyridine-benzimidazole complexes as aquaglyceroporin inhibitors and antiproliferative agents

Brech Aikman,[1,†] Margot N. Wenzel,[1,†] Andreia Mosca,[2,†] Wim T. Klooster,[3] Simon J. Coles,[3] Andreia de Almeida,[1] Graça Soveral,[2,*] Angela Casini[1,*]

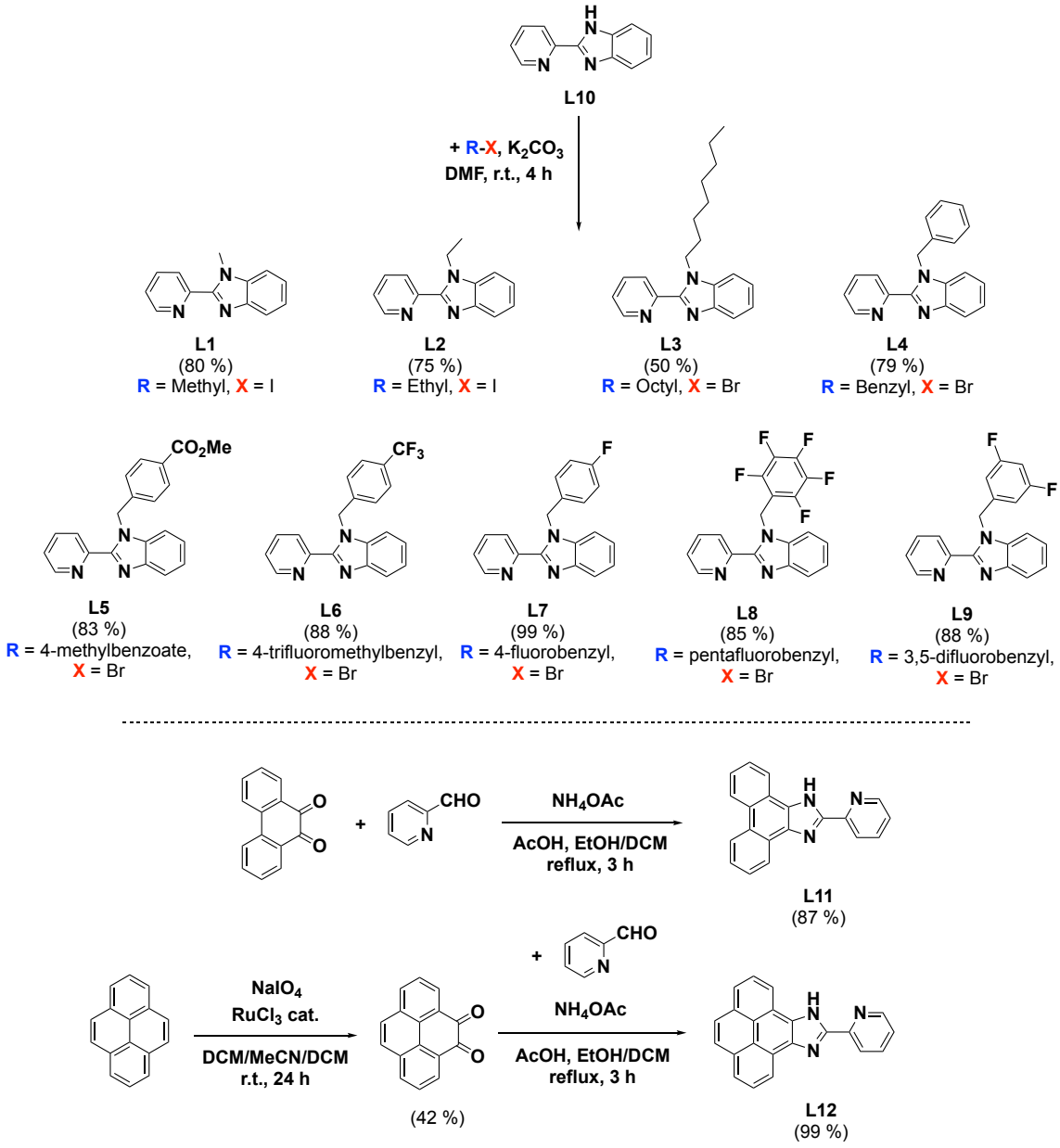

Scheme S1. Synthetic pathways to ligands **L1-L12**.

S1. NMR spectra

Ligand L5

- ^{1}H NMR:

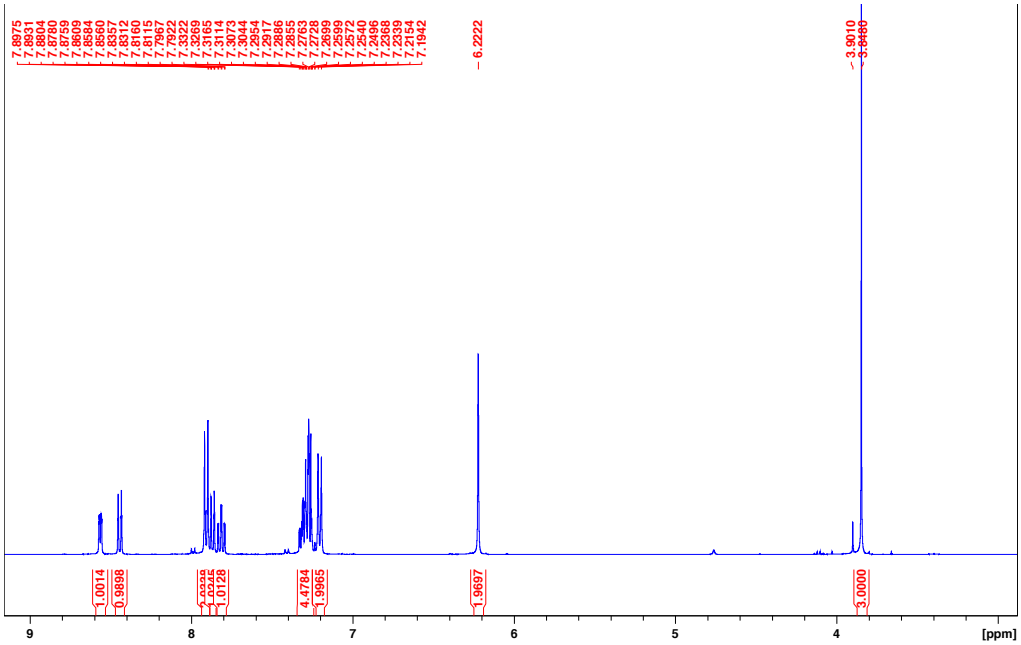

Figure S1. ^{1}H NMR (400.13 MHz, $CDCl_3$) spectrum of ligand **L5**.

- ^{13}C{^{1}H} NMR:

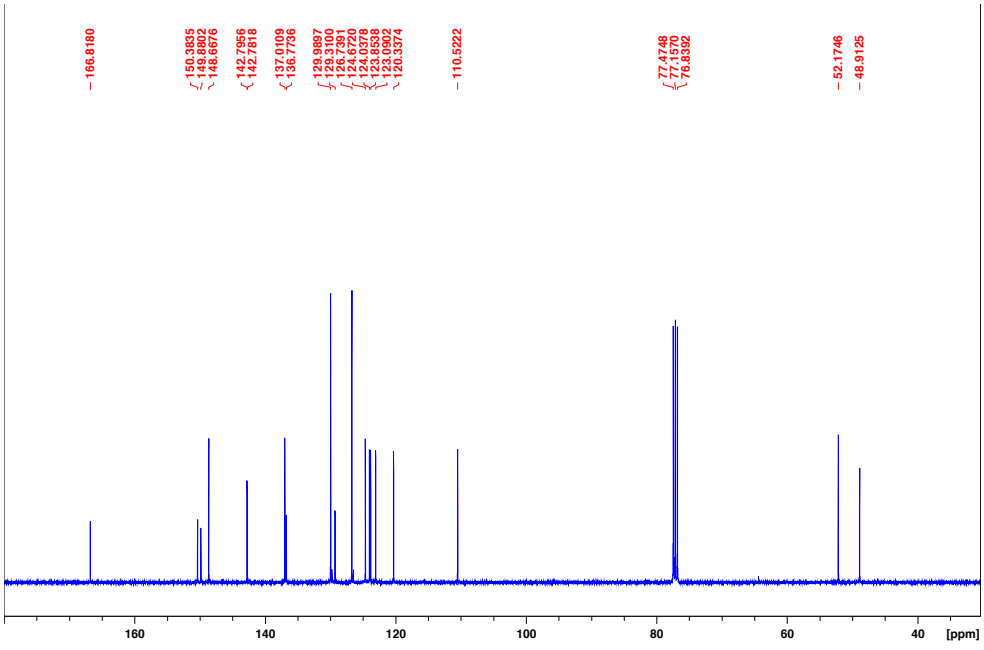

Figure S2. ^{13}C{^{1}H} NMR (100.61 MHz, $CDCl_3$) spectrum of ligand **L5.**

Ligand L6

- ^{1}H NMR:

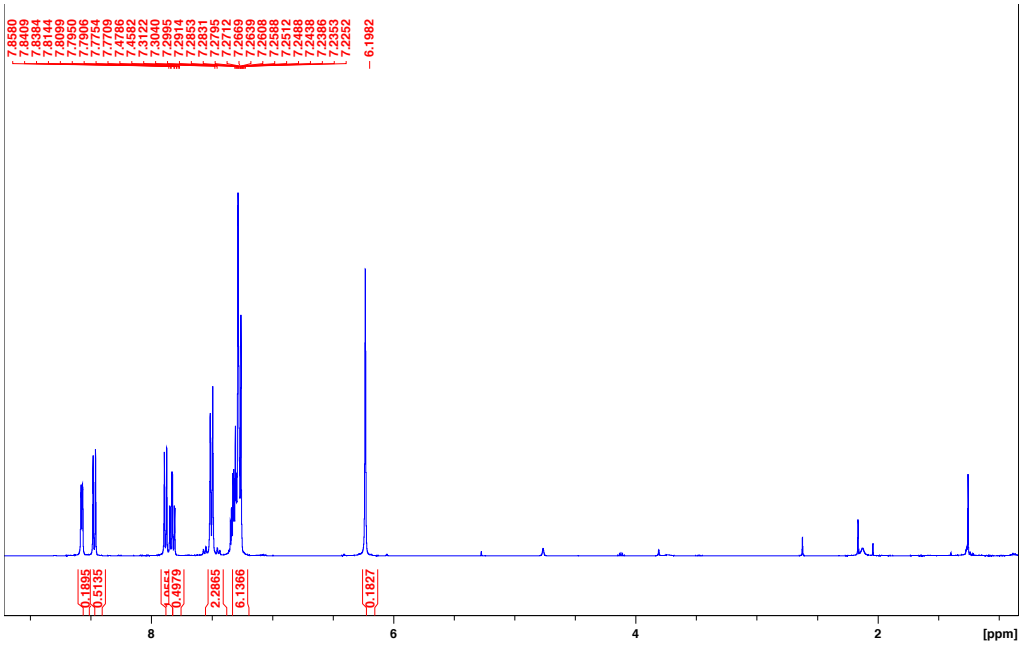

Figure S3. ^{1}H NMR (400.14 MHz, $CDCl_3$) spectrum of ligand **L6.**

- $^{13}C\{^{1}H\}$ NMR:

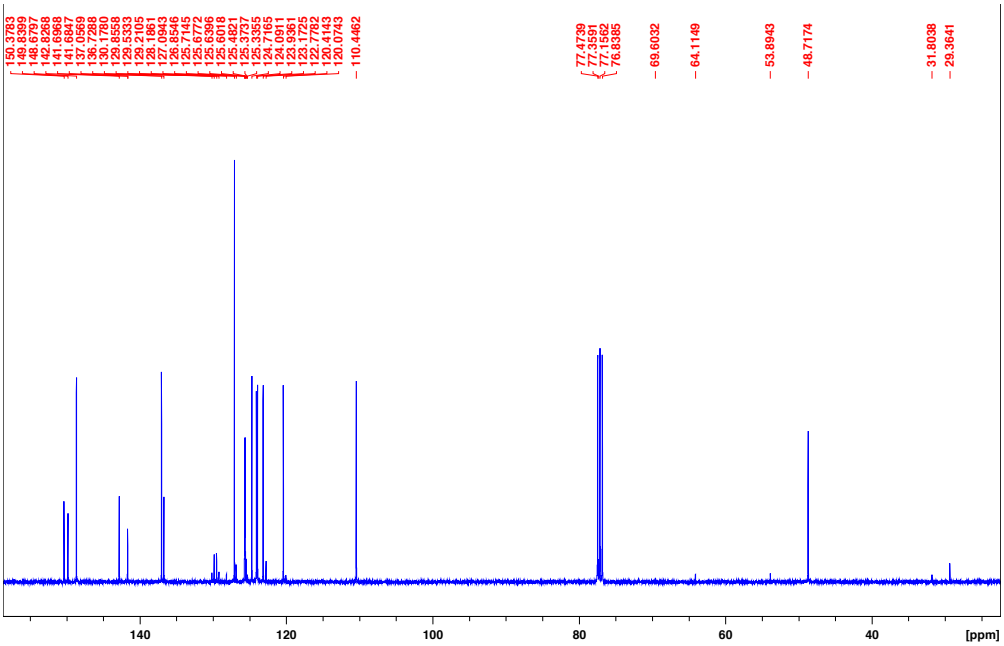

Figure S4. $^{13}C\{^{1}H\}$ NMR (100.61 MHz, $CDCl_3$) spectrum of ligand **L6.**

Complex C2

- ^{1}H NMR:

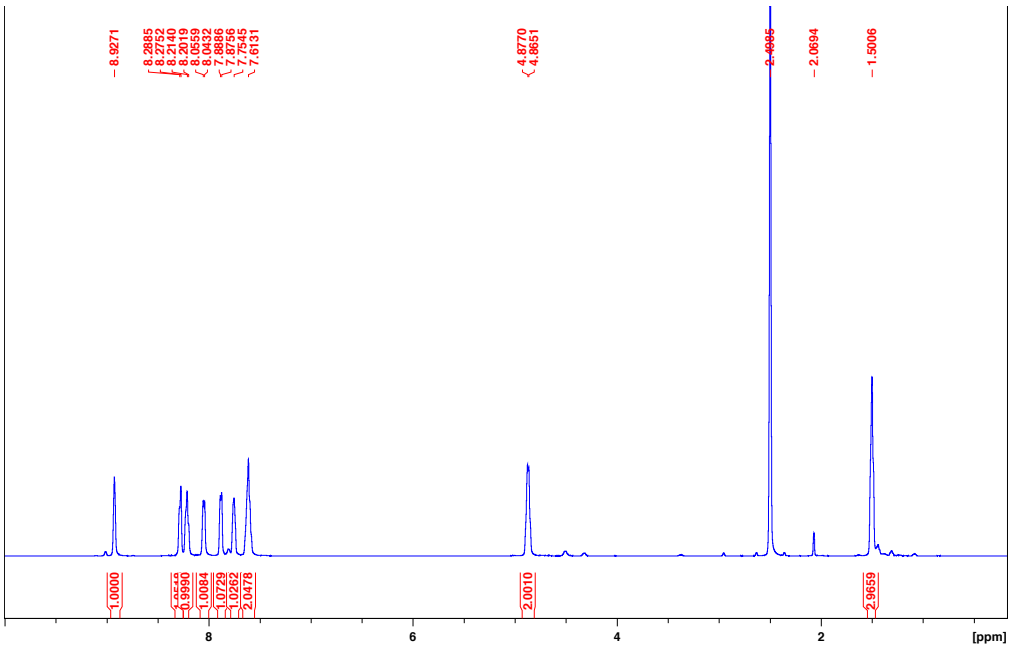

Figure S5. ^{1}H NMR (500.13 MHz, DMSO-d_6) spectrum of complex **C2**.

- ^{13}C{^{1}H} NMR:

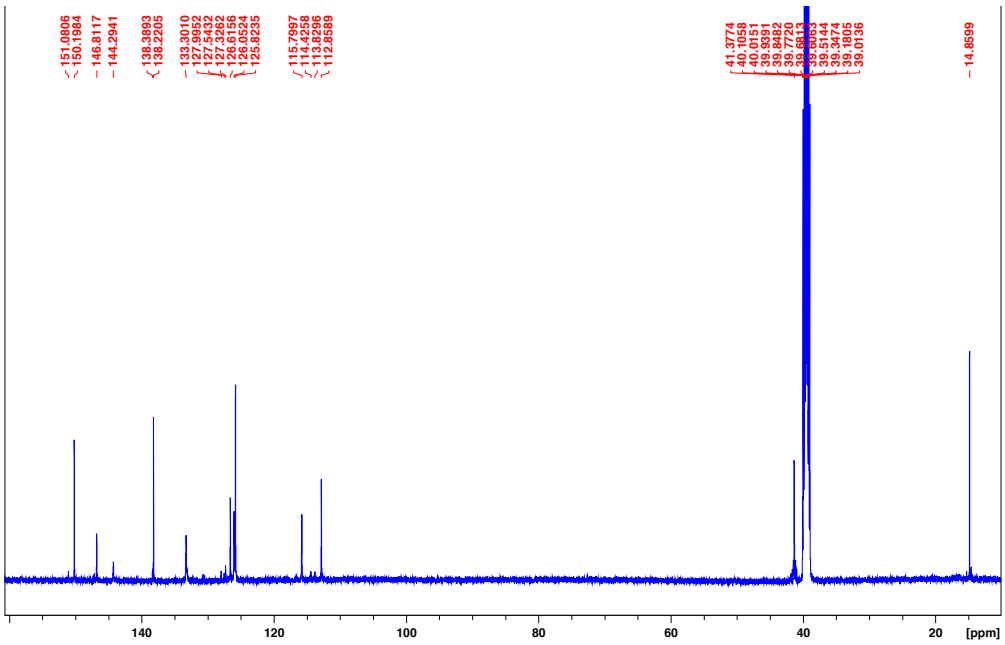

Figure S6. ^{13}C{^{1}H} NMR (125.77 MHz, DMSO-d_6) spectrum of complex **C2.**

Complex C3

- ^{1}H NMR:

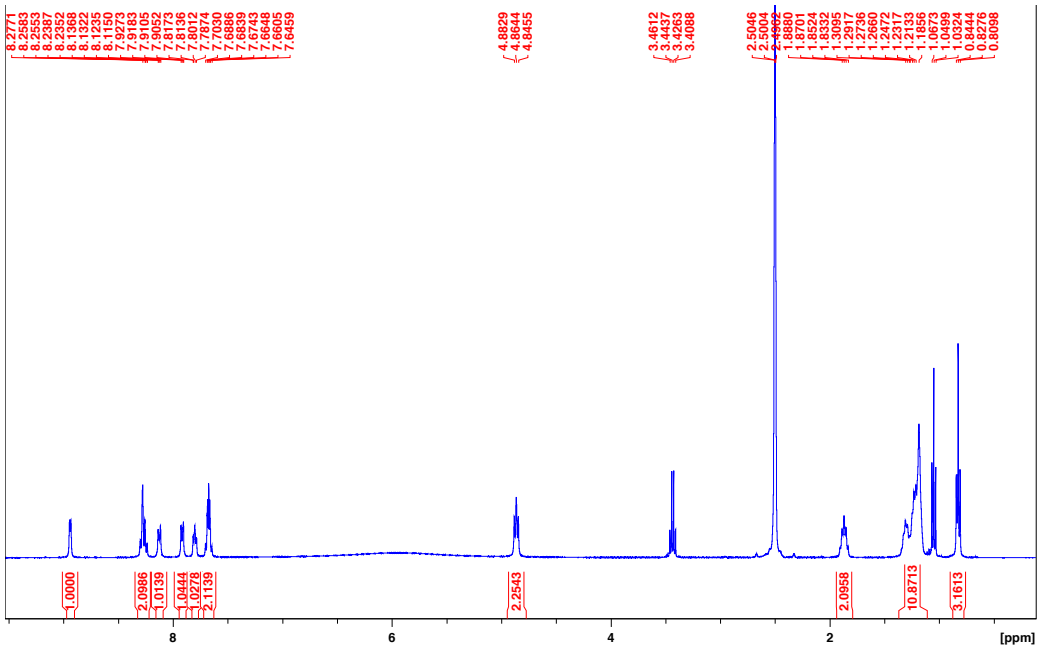

Figure S7. ^{1}H NMR (400.13 MHz, DMSO-d_6) spectrum of complex **C3**.

- ^{13}C{^{1}H} NMR:

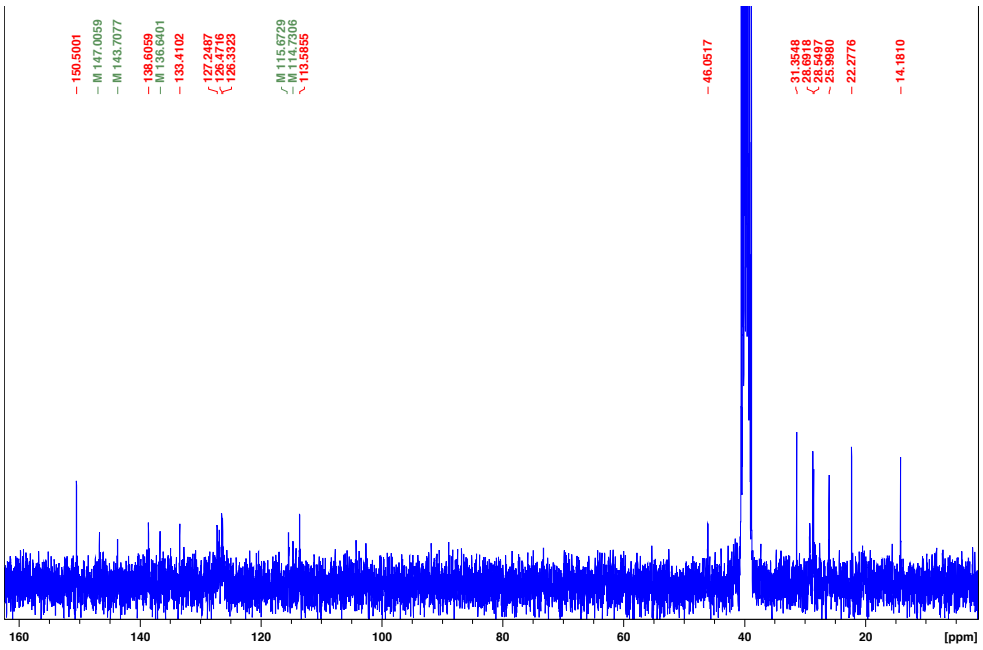

Figure S8. ^{13}C{^{1}H} NMR (125.77 MHz, DMSO-d_6) spectrum of complex **C3**.

Complex C4

- ^{1}H NMR:

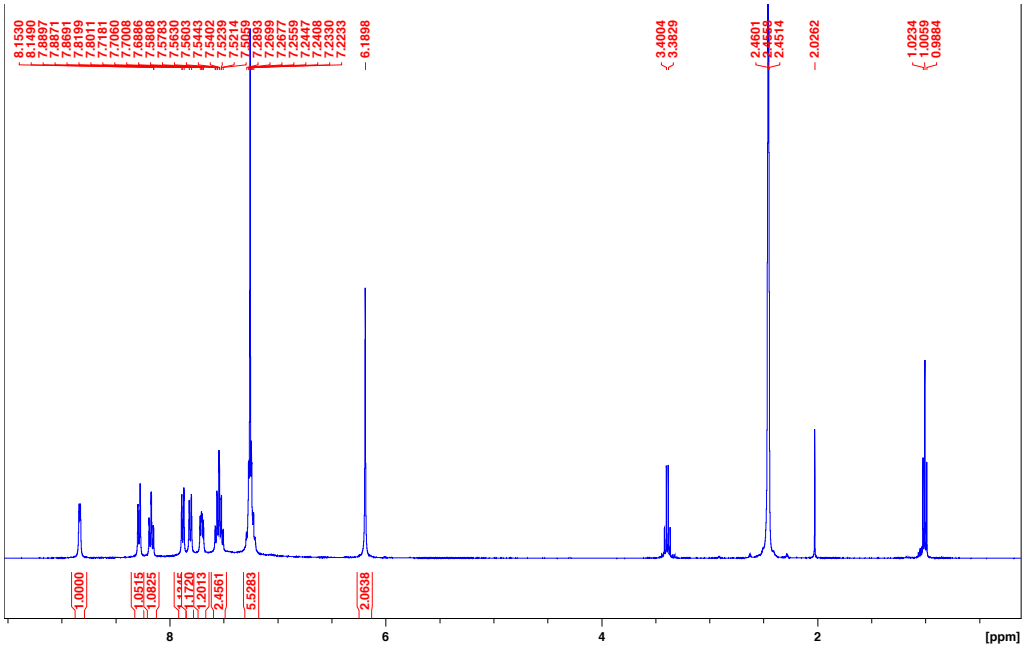

Figure S9. ^{1}H NMR (400.13 MHz, DMSO-d_6) spectrum of complex **C4**.

- ^{13}C{^{1}H} NMR:

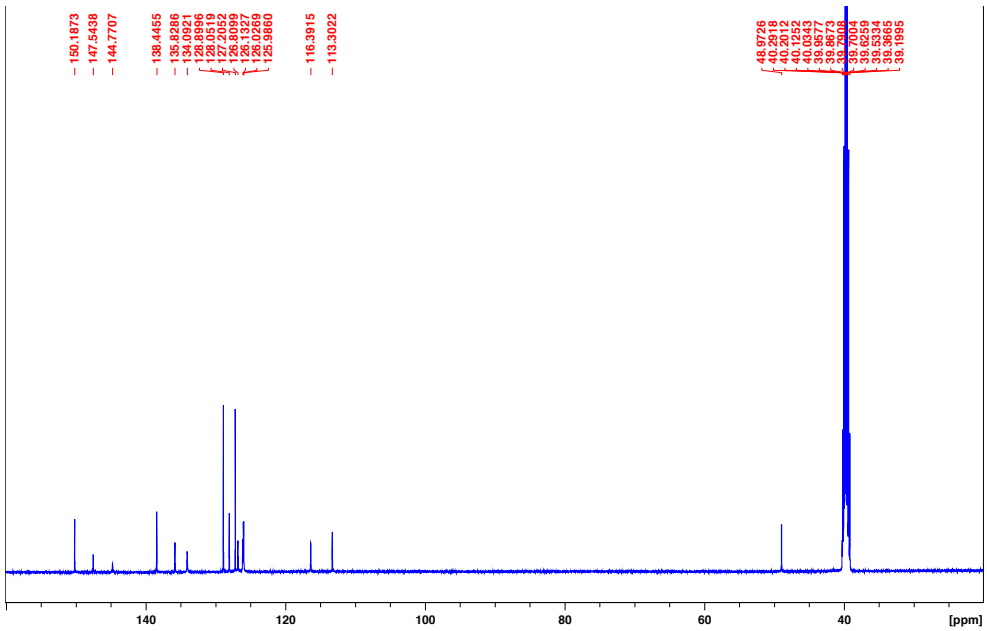

Figure S10. ^{13}C{^{1}H} NMR (125.77 MHz, DMSO-d_6) spectrum of complex **C4**.

Complex C5

- ^{1}H NMR:

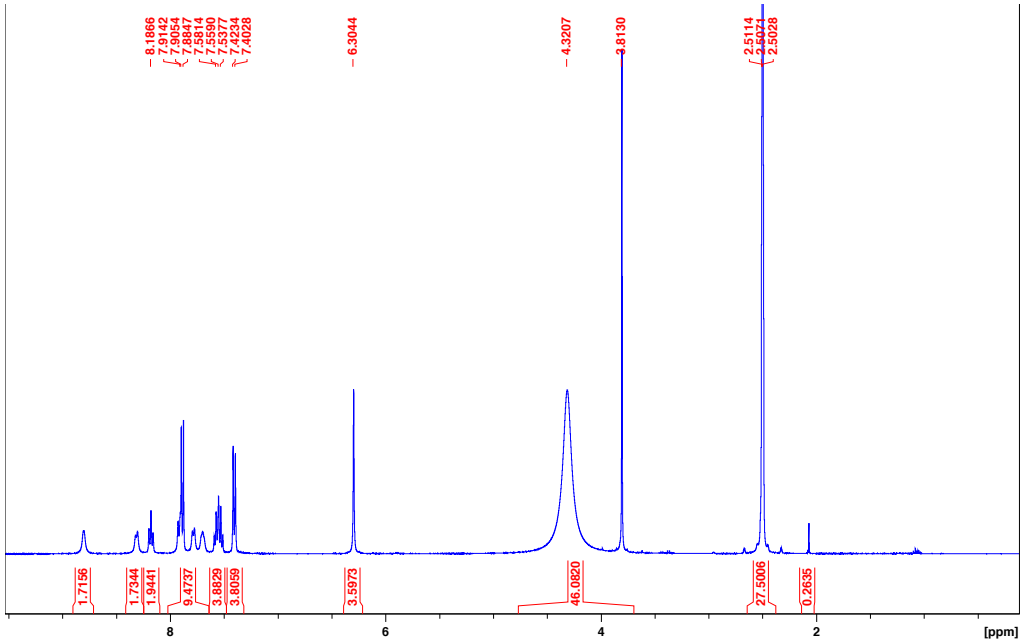

Figure S11. ^{1}H NMR (400.13 MHz, DMSO-d_6) spectrum of complex **C5**.

- ^{13}C{^{1}H} NMR:

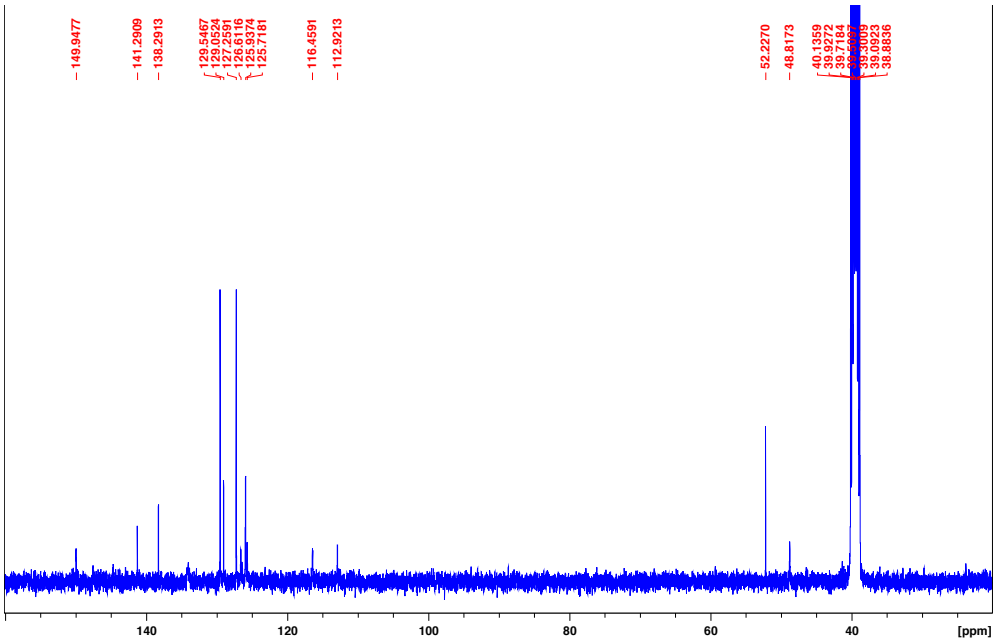

Figure S12. ^{13}C{^{1}H} NMR (100.61 MHz, DMSO-d_6) spectrum of complex **C5**.

Complex C6

- ^{1}H NMR:

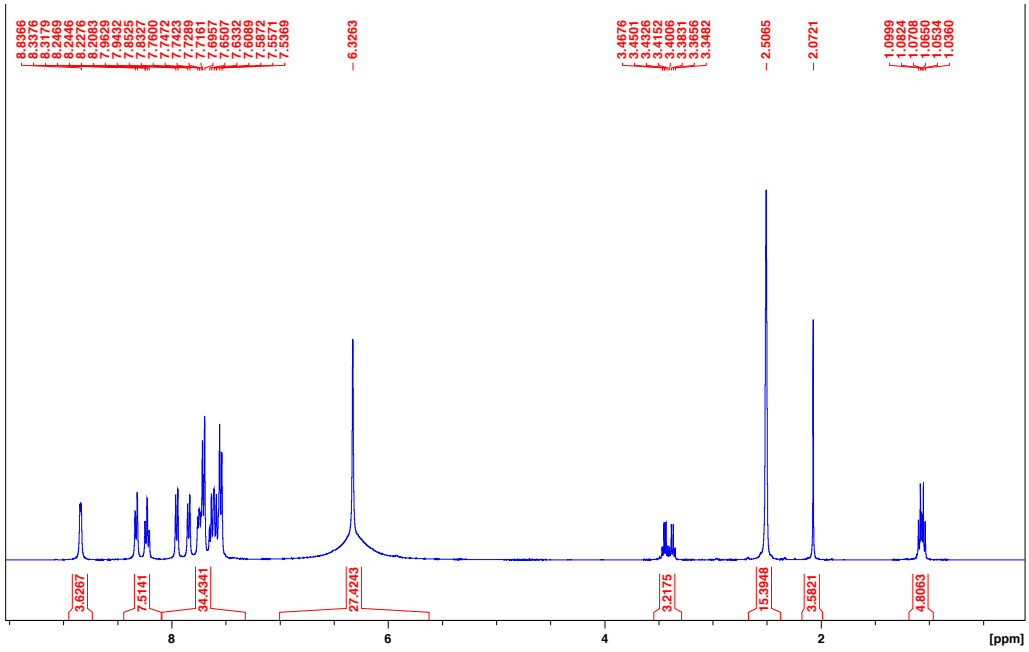

Figure S13. ^{1}H NMR (400.13 MHz, DMSO-d_6) spectrum of complex **C6**.

- ^{13}C{^{1}H} NMR:

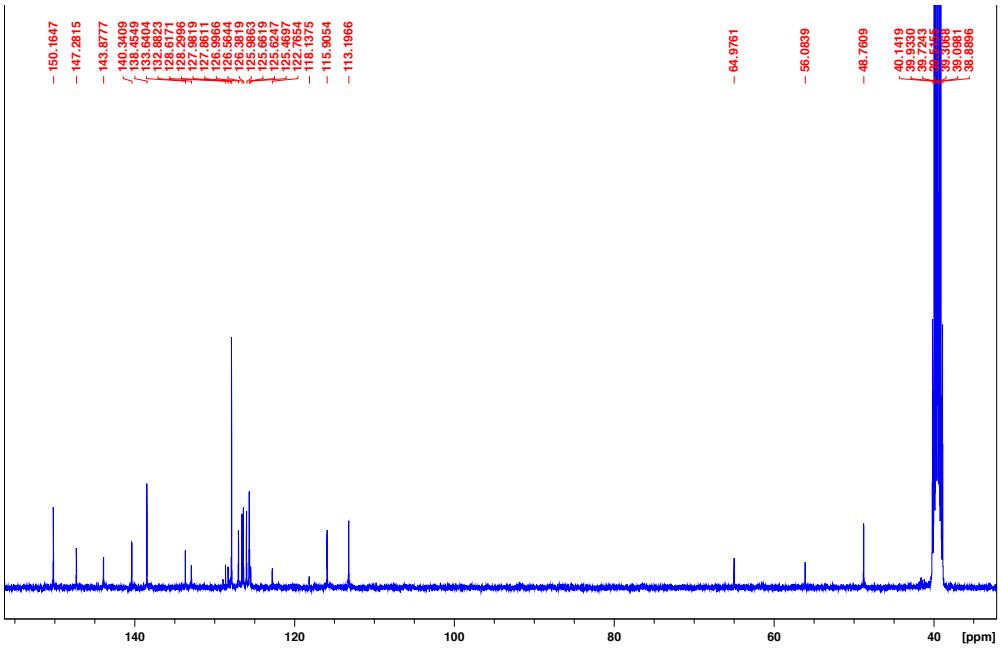

Figure S14. ^{13}C{^{1}H} NMR (100.61 MHz, DMSO-d_6) spectrum of complex **C6**.

Complex C7

- ^{1}H NMR:

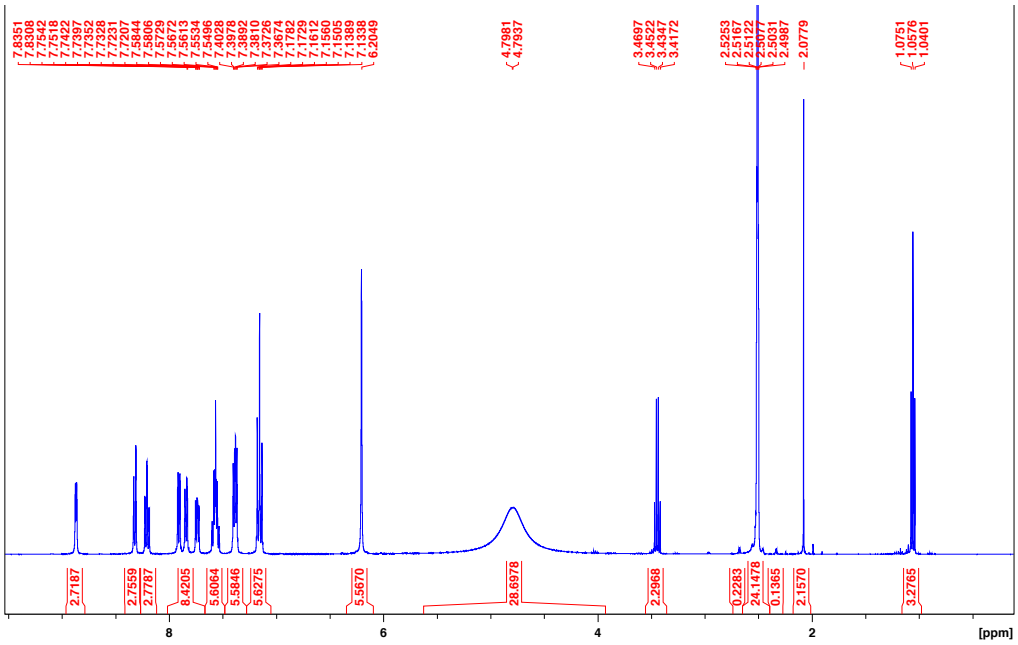

Figure S15. ^{1}H NMR (400.13 MHz, DMSO-d_6) spectrum of complex **C7**.

- ^{13}C{^{1}H} NMR:

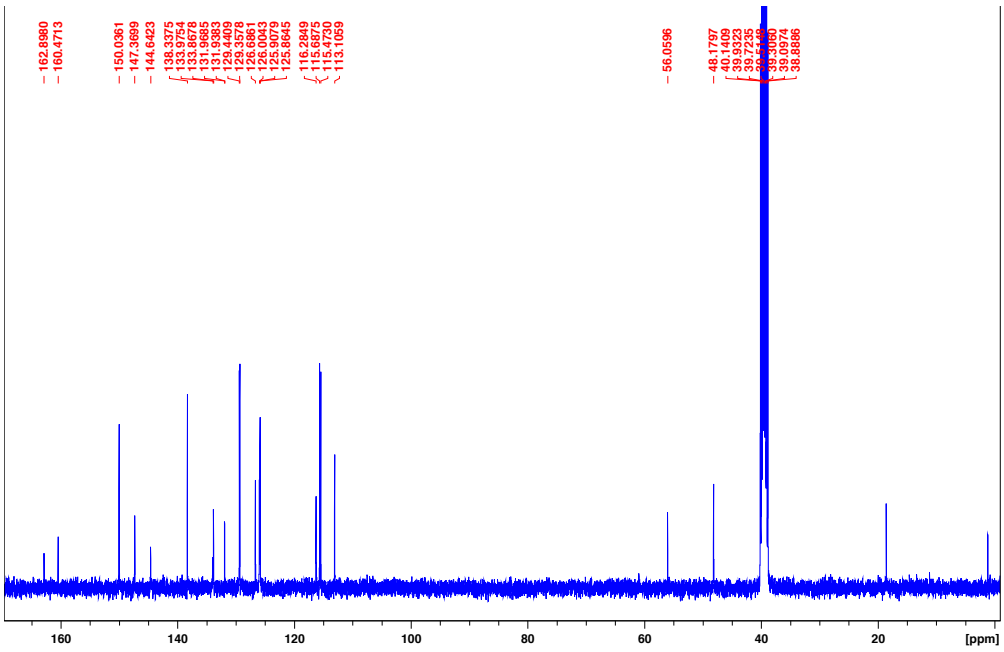

Figure S16. ^{13}C{^{1}H} NMR (100.61 MHz, DMSO-d_6) spectrum of complex **C7**.

Complex C8

- ^{1}H NMR:

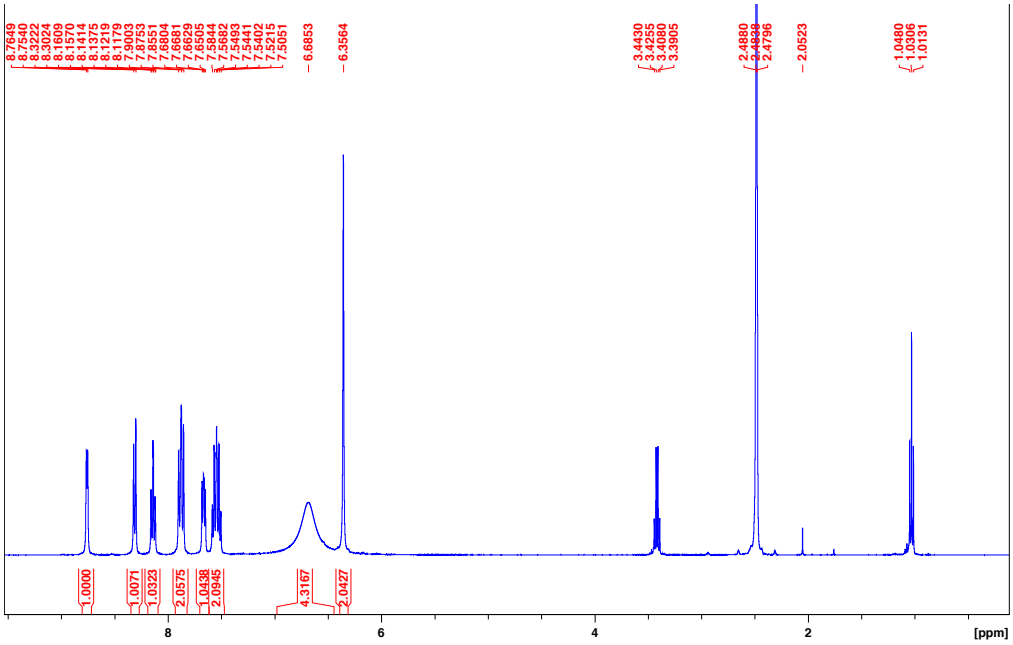

Figure S17. ^{1}H NMR (400.13 MHz, DMSO-d_6) spectrum of complex **C8**.

- ^{13}C{^{1}H} NMR:

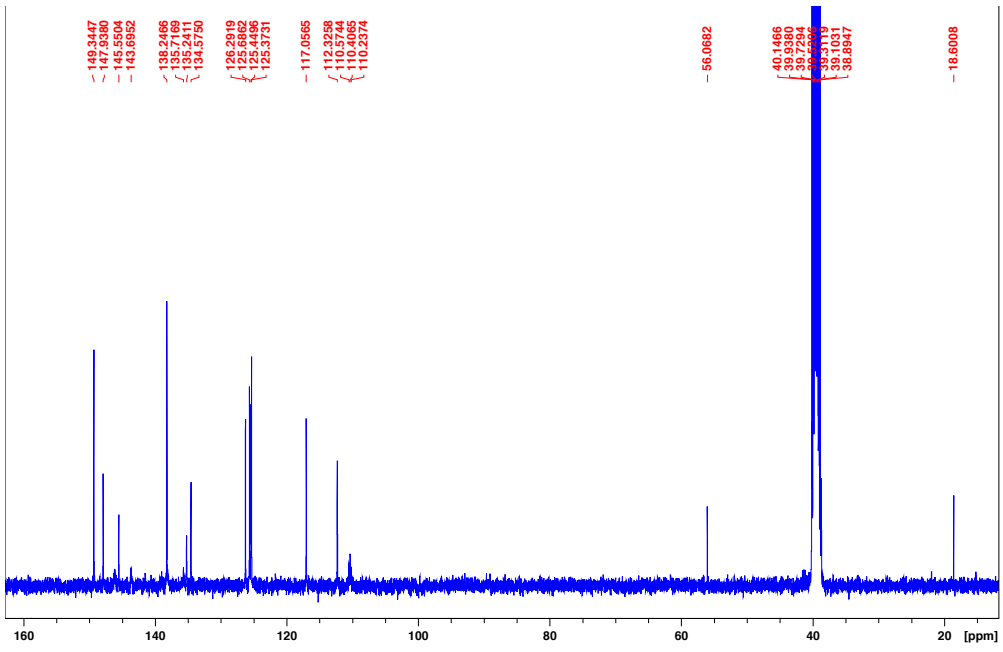

Figure S18. ^{13}C{^{1}H} NMR (100.61 MHz, DMSO-d_6) spectrum of complex **C8**.

Complex C9

- ^{1}H NMR:

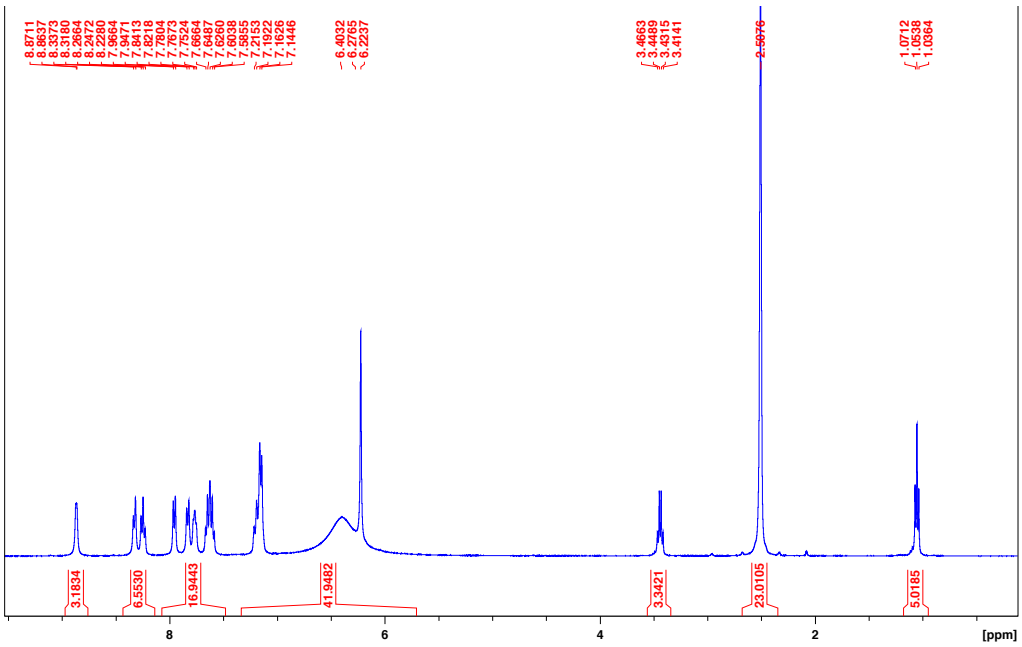

Figure S19. ^{1}H NMR (400.13 MHz, DMSO-d_6) spectrum of complex **C9**.

- ^{13}C{^{1}H} NMR:

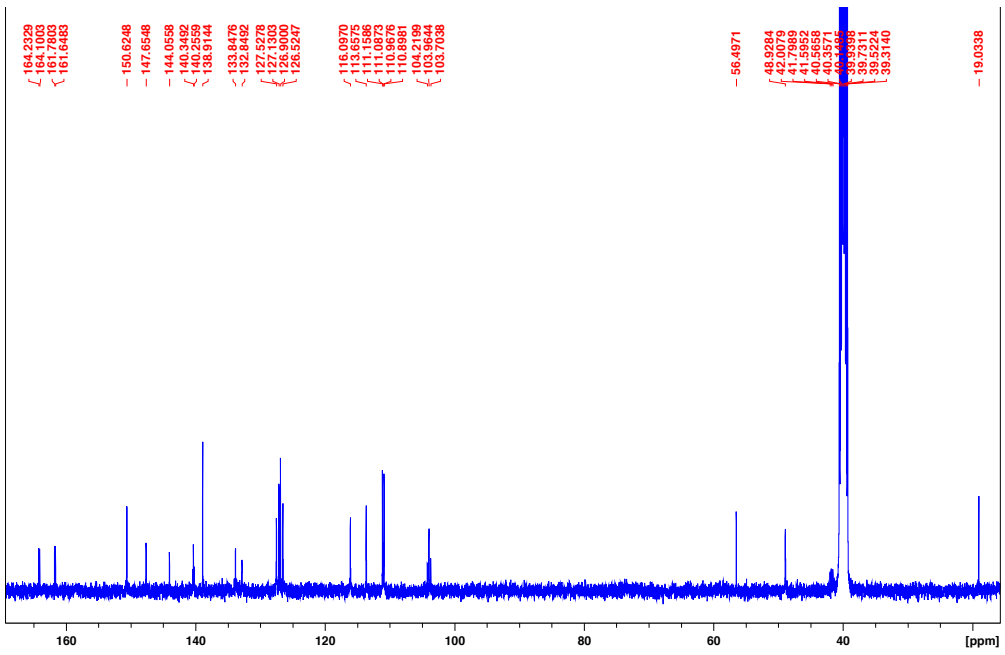

Figure S20. ^{13}C{^{1}H} NMR (100.61 MHz, DMSO-d_6) spectrum of complex **C9**.

Complex 11

- ^{1}H NMR:

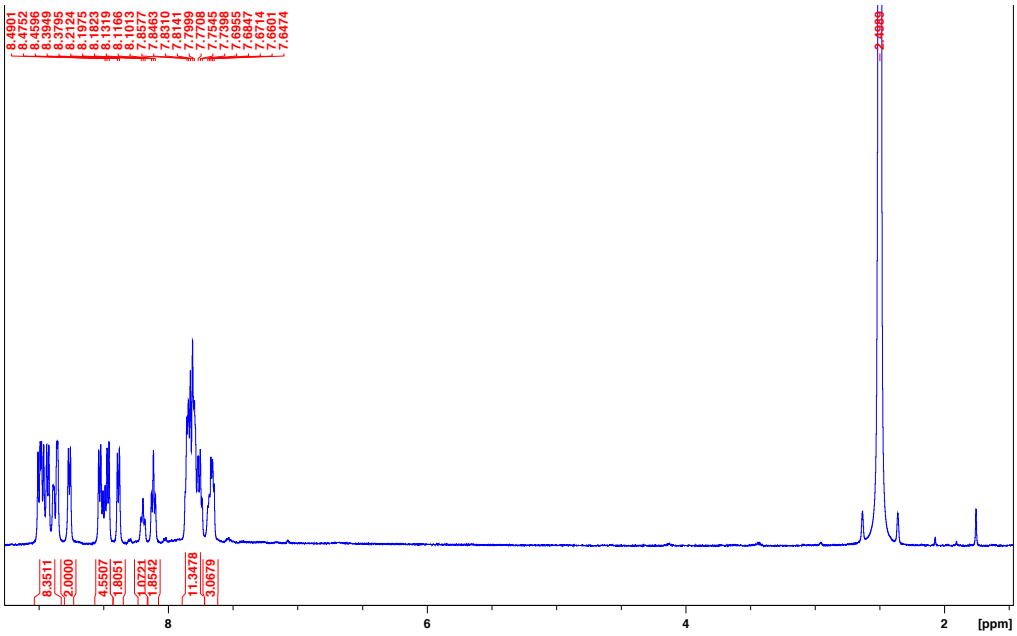

Figure S21. ^{1}H NMR (500.17 MHz, DMSO-d_6) spectrum of complex **C11**.

- ^{13}C{^{1}H} NMR:

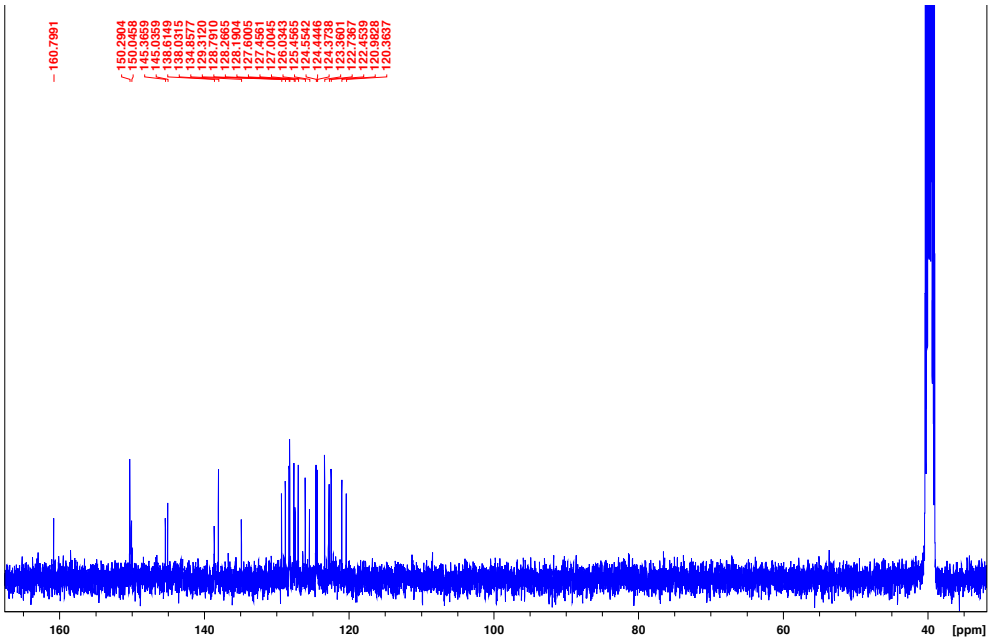

Figure S22. ^{13}C{^{1}H} NMR (125.77 MHz, DMSO-d_6) spectrum of complex **C11**.

Complex 12

- ^{1}H NMR:

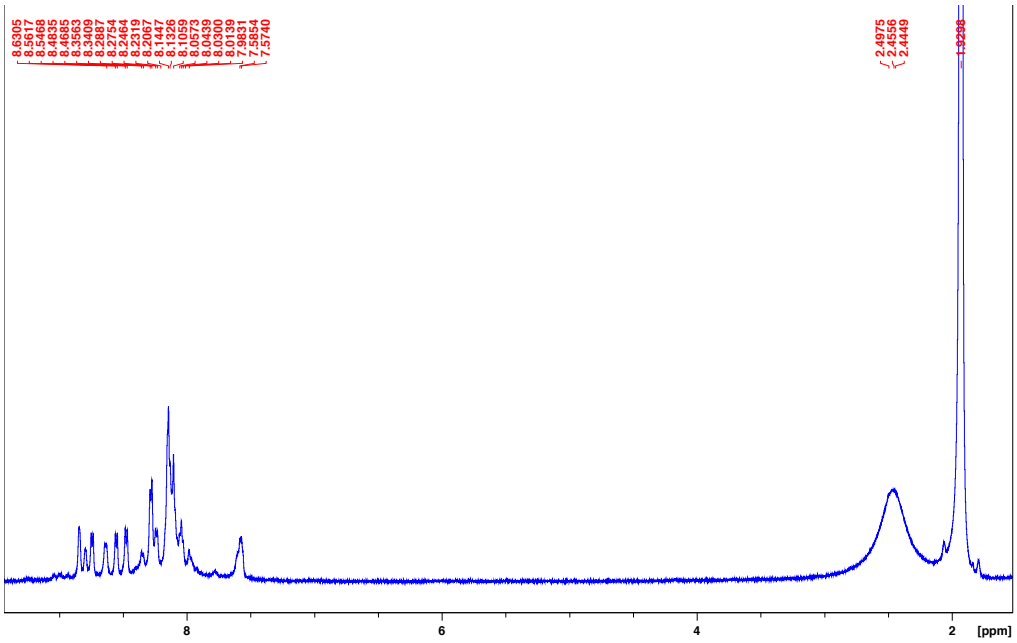

Figure S23. ^{1}H NMR (500.17 MHz, MeCN-d_3) spectrum of complex **C12**.

- ^{13}C{^{1}H} NMR:

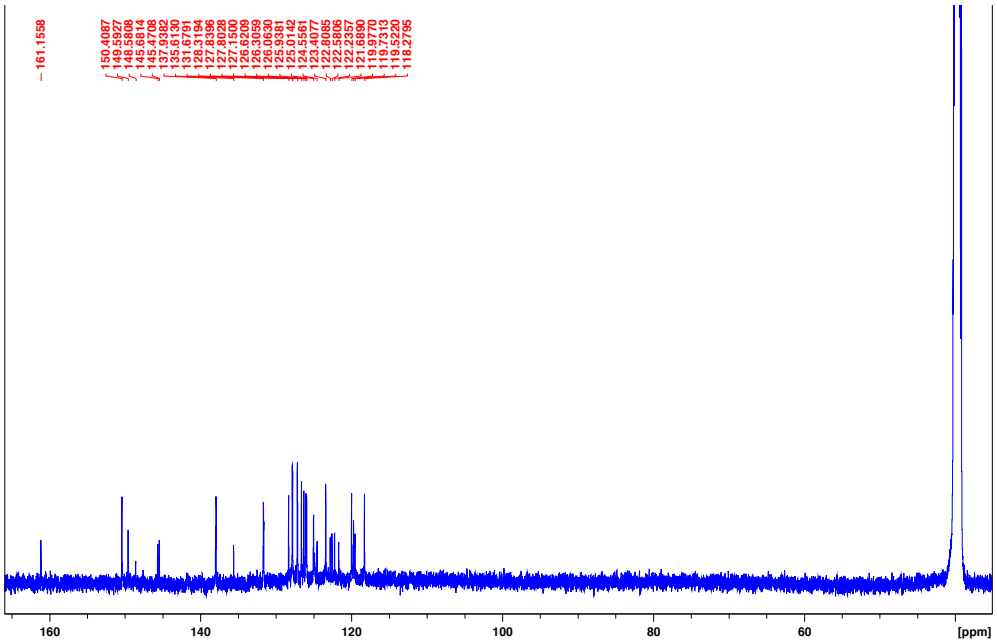

Figure S24. ^{13}C{^{1}H} NMR (125.77 MHz, DMSO-d_6) spectrum of complex **C12**.

S2. Photophysical properties

- **Absorption and emission**

Ligand L1

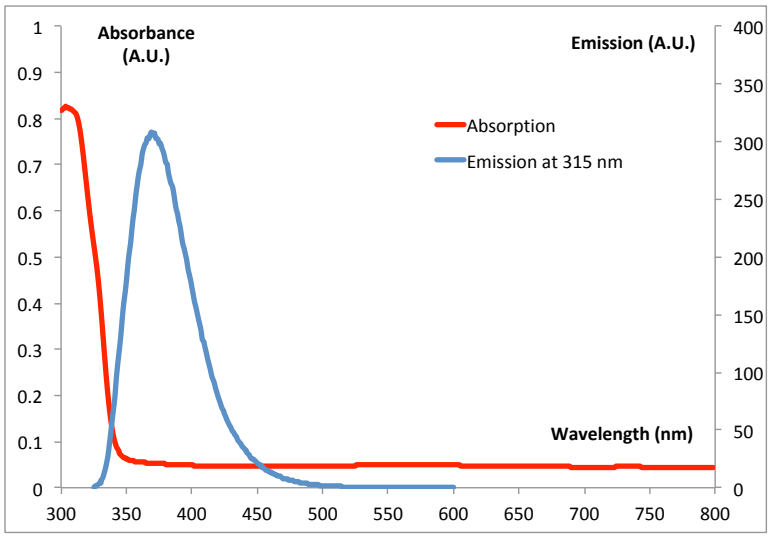

Figure S25: Absorption and emission spectra of ligand **L1**.

Quantum yield in DMSO at 298K: 60%

(Concentration: $3.3.10^{-5}$M)
UV-Vis (DMSO): λ_{max} (nm) (ε, $cm^{-1}.mol^{-1}.dm^3$) 311 (20260).

Complex C1

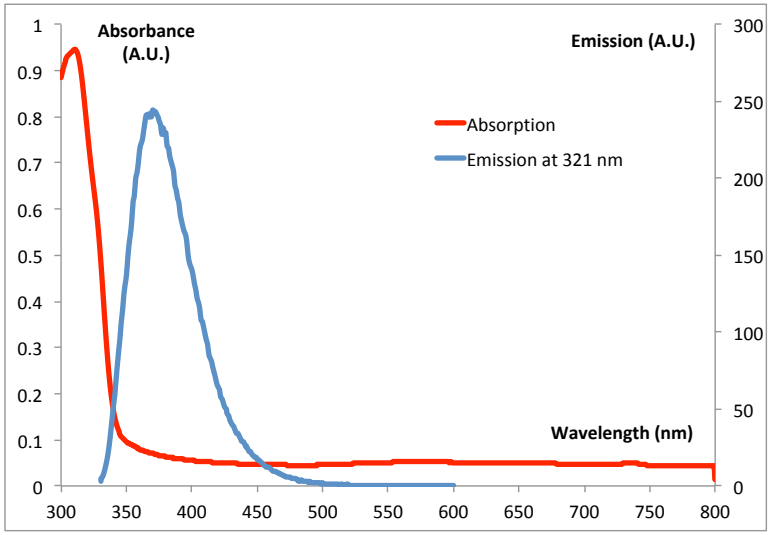

Figure S26: Absorption and emission spectra of complex **C1**.

Quantum yield in DMSO at 298K: 48%
(Concentration: $3.3.10^{-5}$M)
UV-Vis (DMSO): λ_{max} (nm) (ε, $cm^{-1}.mol^{-1}.dm^3$) 311 (23949).

Ligand L2

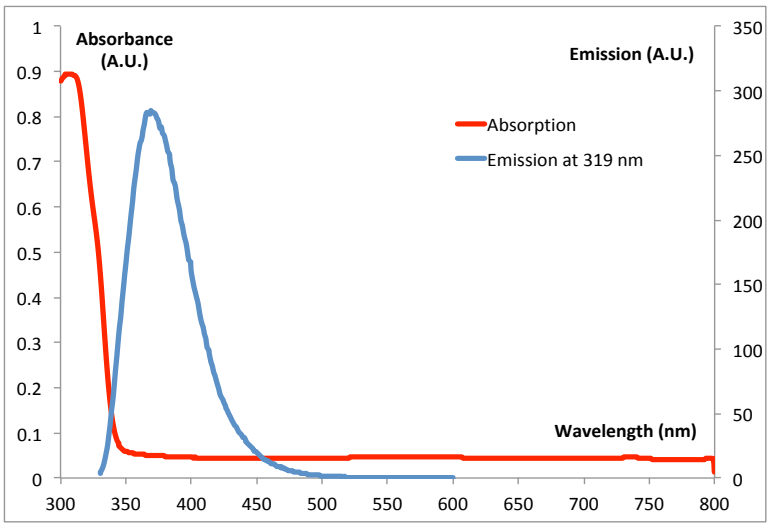

Quantum yield in DMSO at 298K: 54%

(Concentration: $3.3.10^{-5}$M)
UV-Vis (DMSO): λ_{max} (nm) (ε, $cm^{-1}.mol^{-1}.dm^3$) 312 (21645).

Figure S27: Absorption and emission spectra of ligand **L2**.

Complex C2

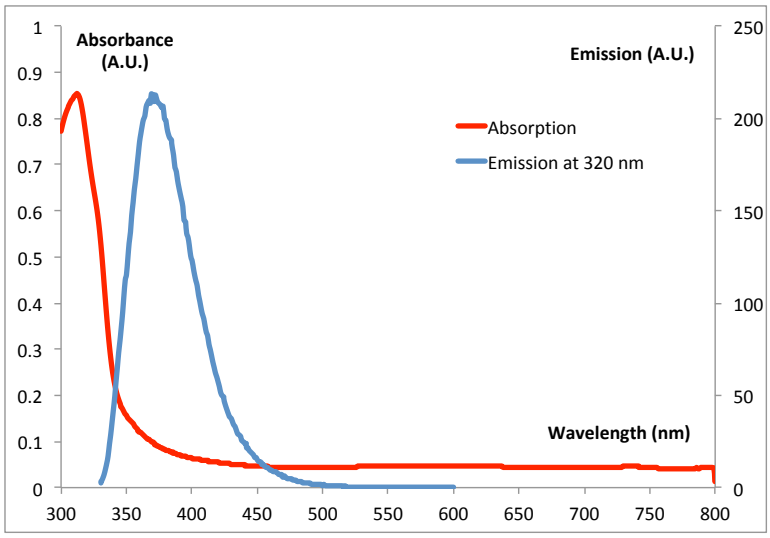

Quantum yield in DMSO at 298K: 39%
(Concentration: $3.3.10^{-5}$M)
UV-Vis (DMSO): λ_{max} (nm) (ε, $cm^{-1}.mol^{-1}.dm^3$) 313 (21654).

Figure S28: Absorption and emission spectra of complex **C2**.

Ligand L3

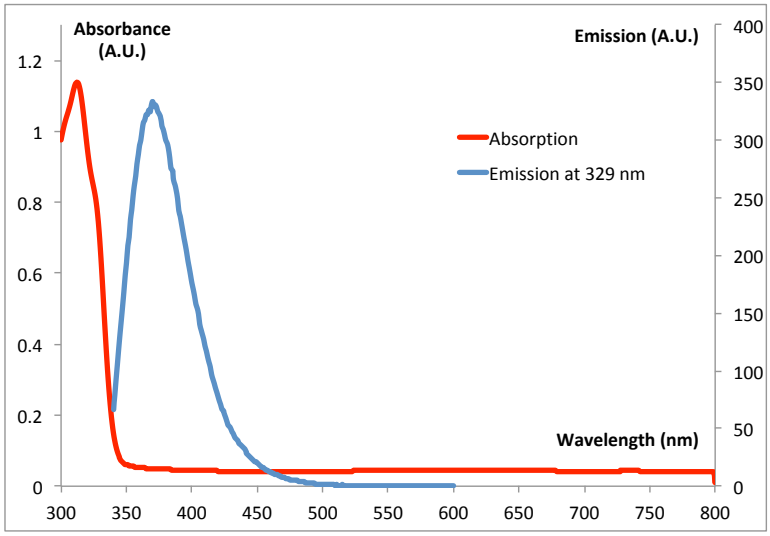

Quantum yield in DMSO at 298K: 50%
(Concentration: $3.3.10^{-5}$M)
UV-Vis (DMSO): λ_{max} (nm) (ε, $cm^{-1}.mol^{-1}.dm^3$) 313 (27357).

Figure S29: Absorption and emission spectra of ligand **L3**.

Complex C3

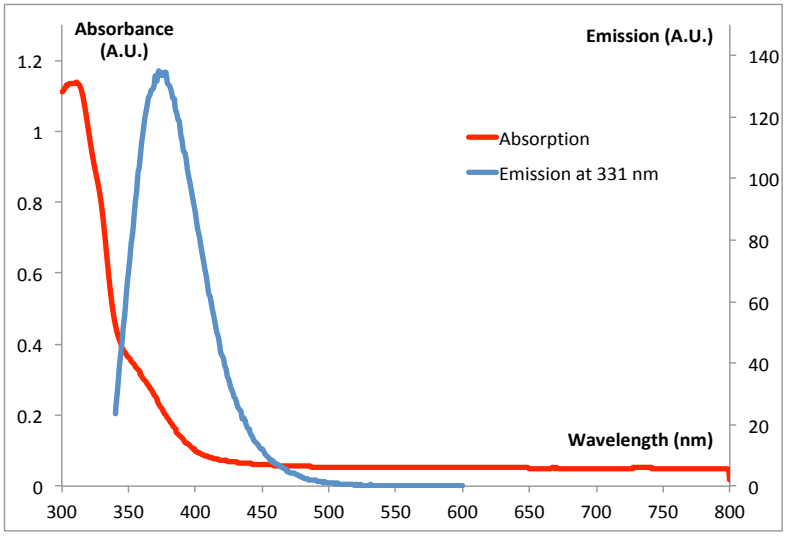

Quantum yield in DMSO at 298K: 27%
(Concentration: $6.6.10^{-5}$M)
UV-Vis (DMSO): λ_{max} (nm) (ε, $cm^{-1}.mol^{-1}.dm^3$) 312 (16006).

Figure S30: Absorption and emission spectra of complex **C3**.

Ligand L4

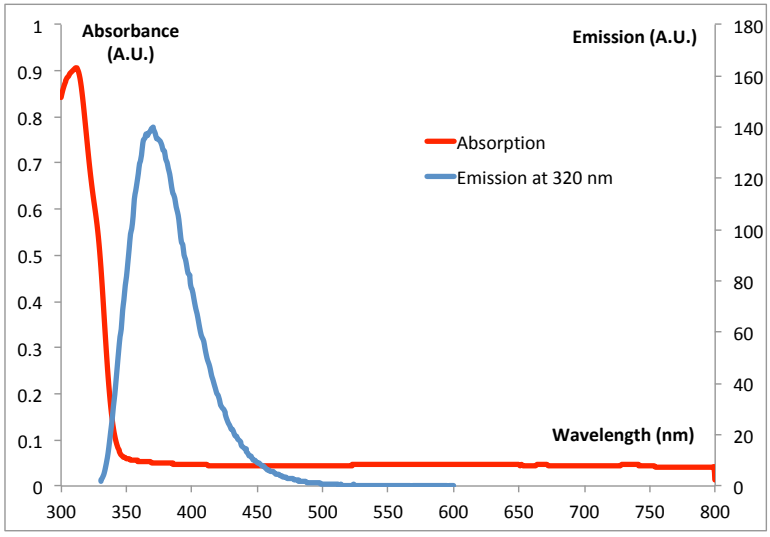

Quantum yield in DMSO at 298K: 27%

(Concentration: $3.3.10^{-5}$M)
UV-Vis (DMSO): λ_{max} (nm) (ε, $cm^{-1}.mol^{-1}.dm^3$) 312 (24729).

Figure S31: Absorption and emission spectra of ligand **L4**.

Complex C4

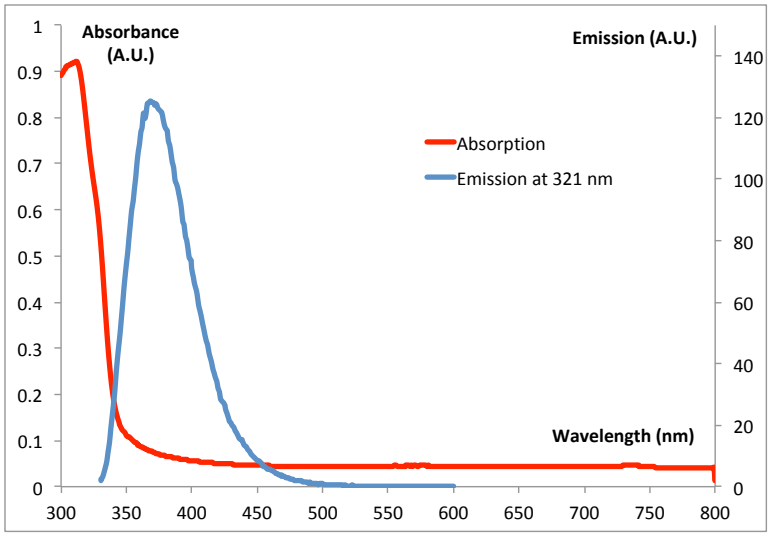

Quantum yield in DMSO at 298K: 23%

(Concentration: $3.3.10^{-5}$M)
UV-Vis (DMSO): λ_{max} (nm) (ε, $cm^{-1}.mol^{-1}.dm^3$) 313 (21527).

Figure S32: Absorption and emission spectra of complex **C4**.

Ligand L5

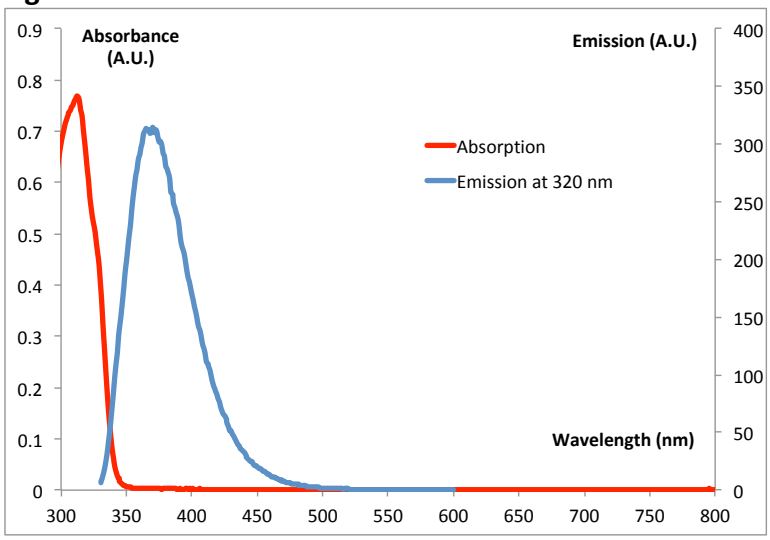

Quantum yield in DMSO at 298K: 30%

(Concentration: $4.2.10^{-5}$M)
UV-Vis (DMSO): λ_{max} (nm) (ε, $cm^{-1}.mol^{-1}.dm^3$) 313 (14123).

Figure S33: Absorption and emission spectra of ligand **L5**.

Complex C5

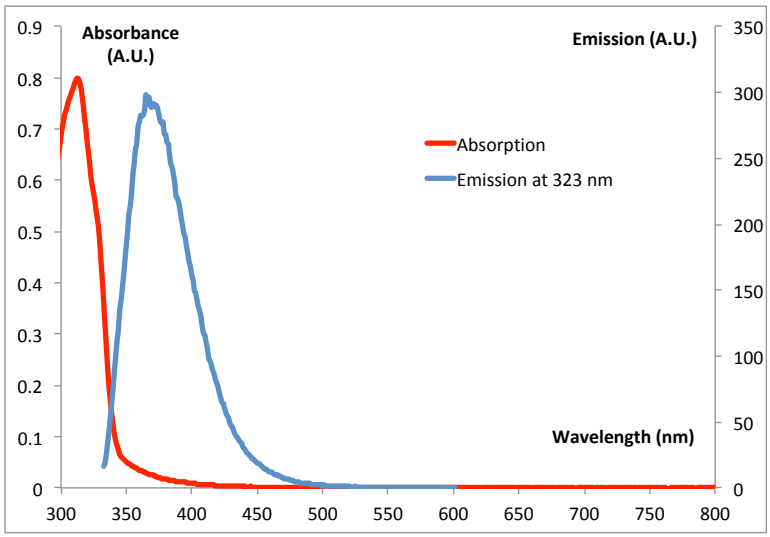

Quantum yield in DMSO at 298K: 29%

(Concentration: $3.4.10^{-5}$M)
UV-Vis (DMSO): λ_{max} (nm) (ε, $cm^{-1}.mol^{-1}.dm^3$) 312 (23448).

Figure S34: Absorption and emission spectra of complex **C5**.

Ligand L6

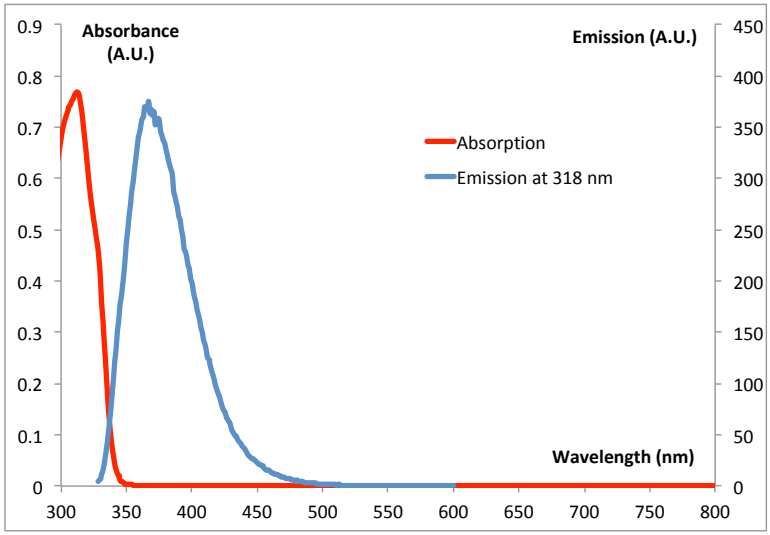

Quantum yield in DMSO at 298K: 38%

(Concentration: $3.3.10^{-5}$M)
UV-Vis (DMSO): λ_{max} (nm) (ε, $cm^{-1}.mol^{-1}.dm^3$) 313 (23130).

Figure S35: Absorption and emission spectra of ligand **L6**.

Complex C6

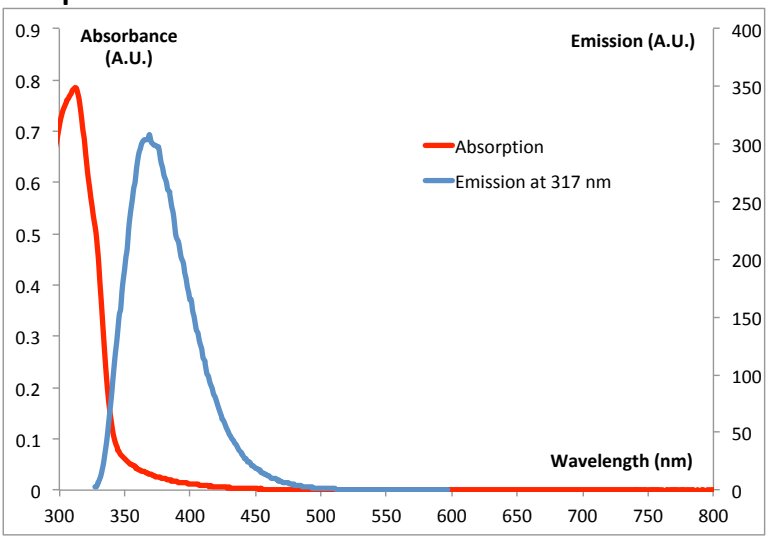

Quantum yield in DMSO at 298K: 32%

(Concentration: $2.7.10^{-5}$M)
UV-Vis (DMSO): λ_{max} (nm) (ε, $cm^{-1}.mol^{-1}.dm^3$) 312 (24699).

Figure S36: Absorption and emission spectra of complex **C6**.

Ligand L7

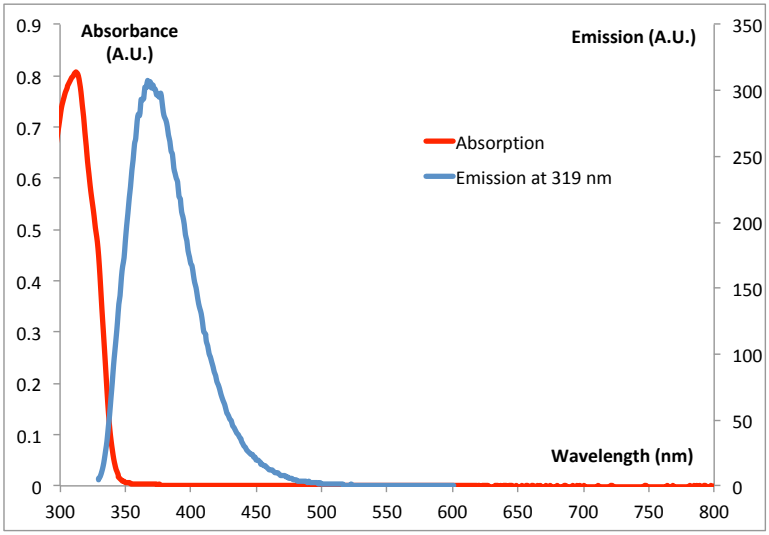

Quantum yield in DMSO at 298K: 32%

(Concentration: $3.8.10^{-5}$M)
UV-Vis (DMSO): λ_{max} (nm) (ε, $cm^{-1}.mol^{-1}.dm^3$) 312 (21244).

Figure S37: Absorption and emission spectra of ligand **L7**.

Complex C7

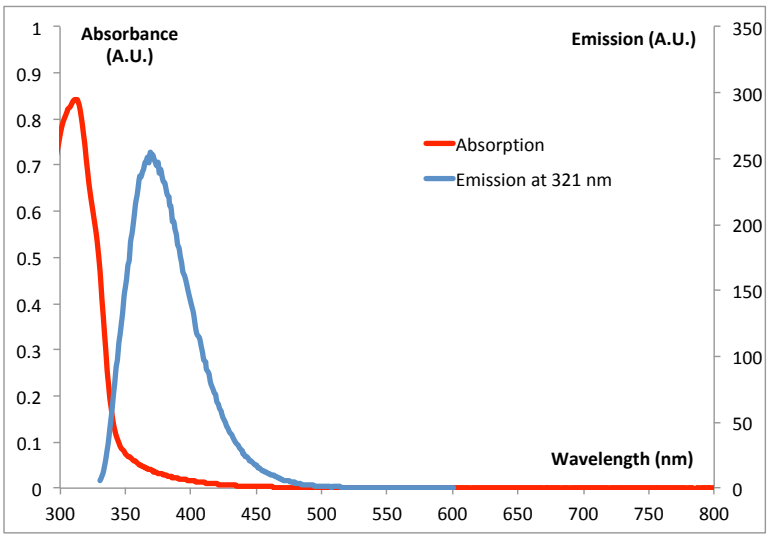

Quantum yield in DMSO at 298K: 26%

(Concentration: $2.6.10^{-5}$M)
UV-Vis (DMSO): λ_{max} (nm) (ε, $cm^{-1}.mol^{-1}.dm^3$) 312 (25542).

Figure S38: Absorption and emission spectra of complex **C7**.

Ligand L8

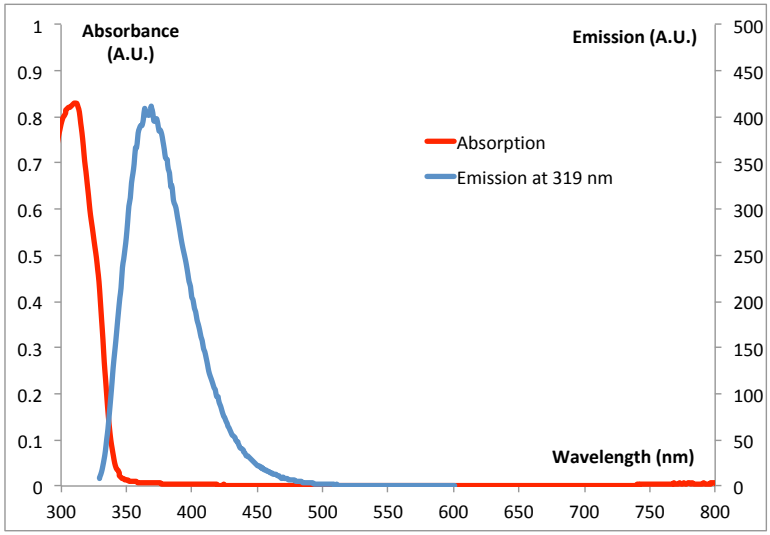

Quantum yield in DMSO at 298K: 42%
(Concentration: $2.4.10^{-5}$M)
UV-Vis (DMSO): λ_{max} (nm) (ε, $cm^{-1}.mol^{-1}.dm^3$) 312 (29031).

Figure S39: Absorption and emission spectra of ligand **L8**.

Complex C8

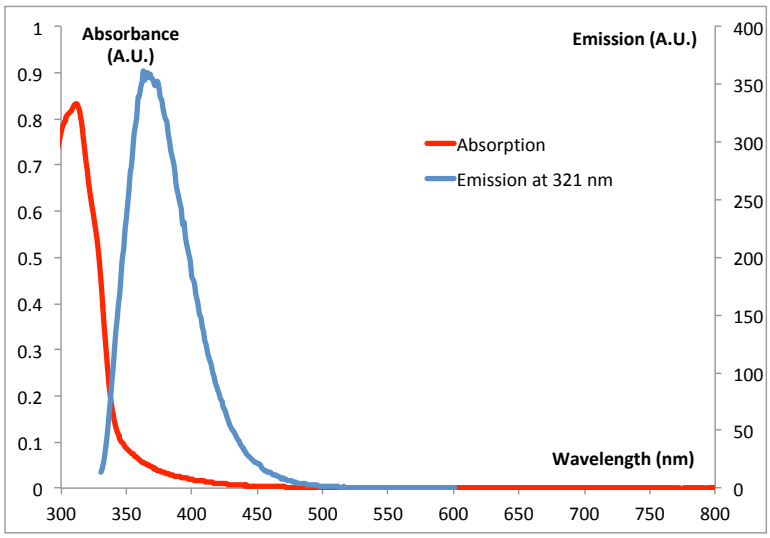

Quantum yield in DMSO at 298K: 36%
(Concentration: $2.9.10^{-5}$M)
UV-Vis (DMSO): λ_{max} (nm) (ε, $cm^{-1}.mol^{-1}.dm^3$) 311 (23441).

Figure S40: Absorption and emission spectra of complex **C8**.

Ligand L9

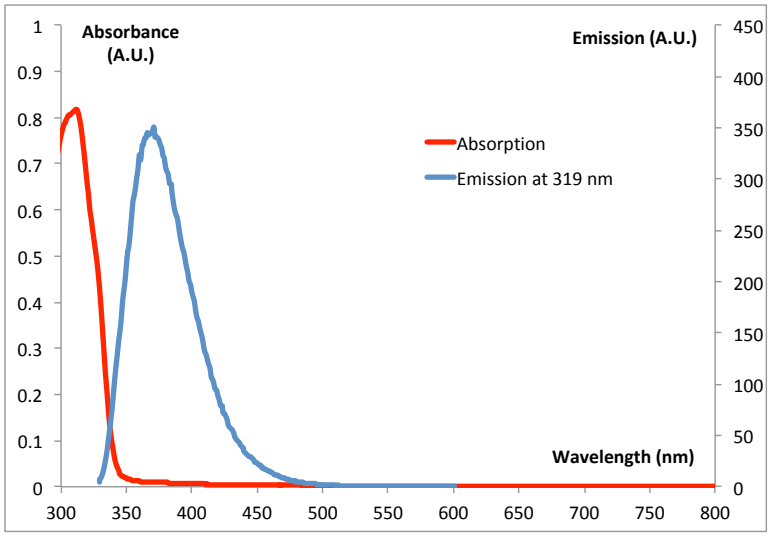

Quantum yield in DMSO at 298K: 36%
(Concentration: $3.1.10^{-5}$M)
UV-Vis (DMSO): λ_{max} (nm) (ε, $cm^{-1}.mol^{-1}.dm^3$) 312 (22425).

Figure S41: Absorption and emission spectra of ligand **L9**.

Complex C9

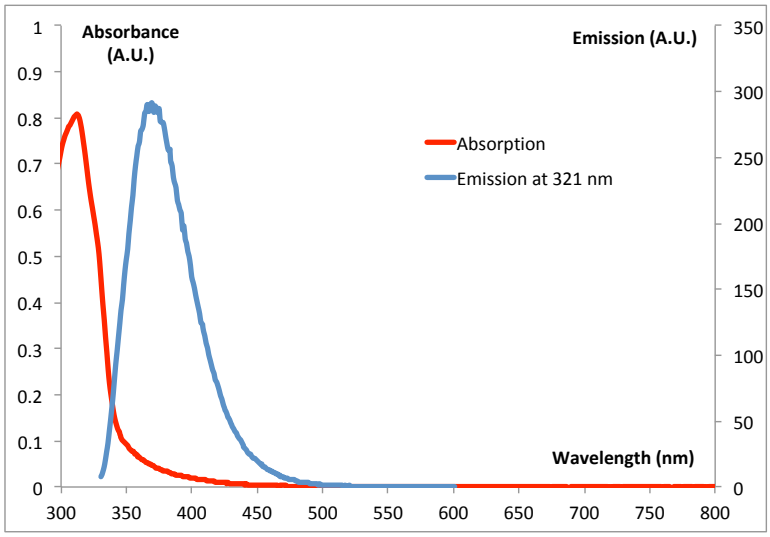

Quantum yield in DMSO at 298K: 30%

(Concentration: $3.0.10^{-5}$M)
UV-Vis (DMSO): λ_{max} (nm) (ε, $cm^{-1}.mol^{-1}.dm^3$) 313 (14367).

Figure S42: Absorption and emission spectra of complex **C9**.

Ligand L10

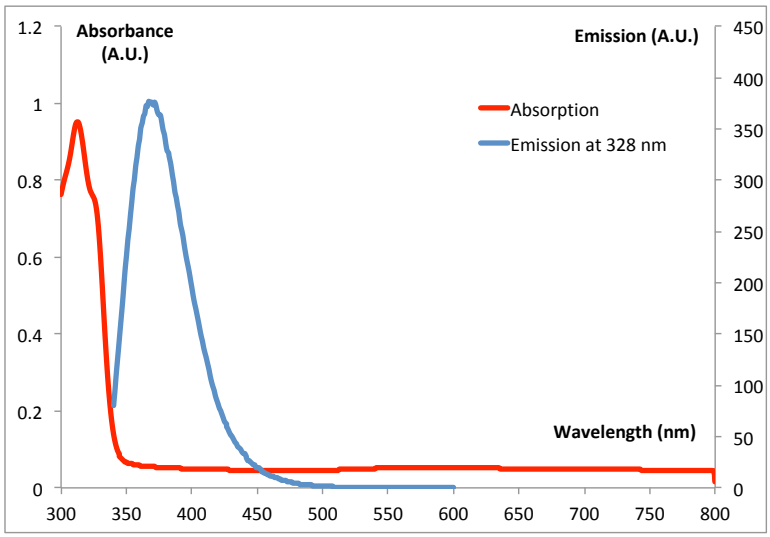

Quantum yield in DMSO at 298K: 69%

(Concentration: $3.3.10^{-5}$M)
UV-Vis (DMSO): λ_{max} (nm) (ε, $cm^{-1}.mol^{-1}.dm^3$) 313 (24475).

Figure S43: Absorption and emission spectra of ligand **L10**.

Complex C10

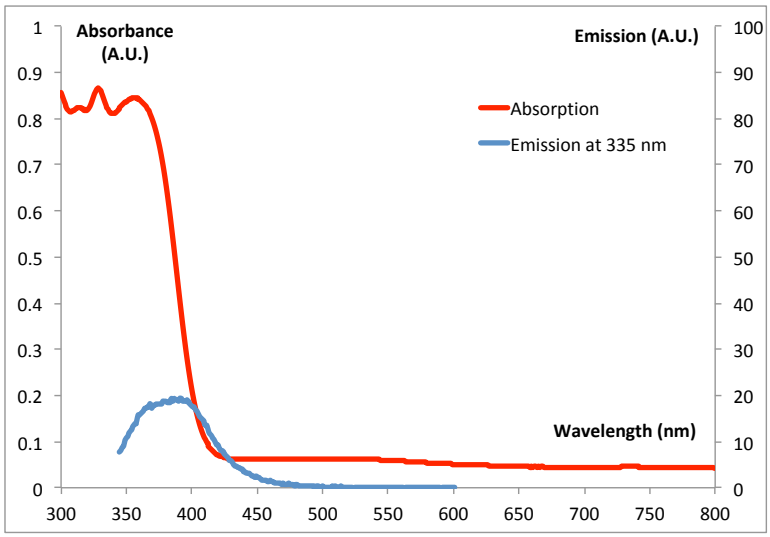

Quantum yield in DMSO at 298K: 4%

(Concentration: $5.0.10^{-5}$M)
UV-Vis (DMSO): λ_{max} (nm) (ε, $cm^{-1}.mol^{-1}.dm^3$) 328 (12883).

Figure S44: Absorption and emission spectra of complex **C10**.

Ligand L11

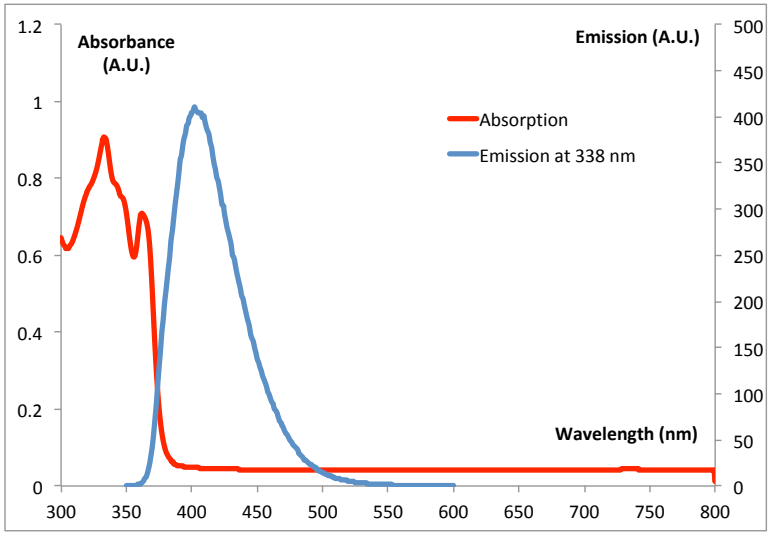

Quantum yield in DMSO at 298K: 74%
(Concentration: $4.0.10^{-5}$M)
UV-Vis (DMSO): λ_{max} (nm) (ε, $cm^{-1}.mol^{-1}.dm^3$) 333 (20088), 362 (15966).

Figure S45: Absorption and emission spectra of ligand **L11**.

Complex C11

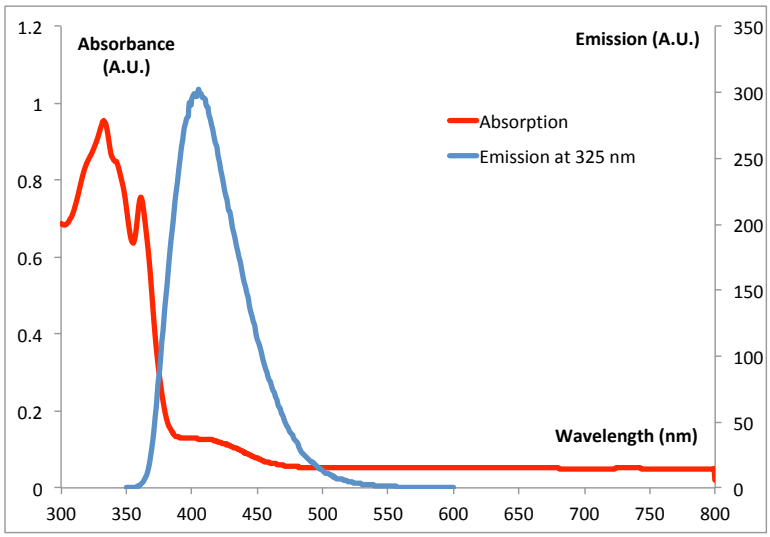

Quantum yield in DMSO at 298K: 56%
(Concentration: $5.6.10^{-5}$M)
UV-Vis (DMSO): λ_{max} (nm) (ε, $cm^{-1}.mol^{-1}.dm^3$) 333 (20891), 362 (16528).

Figure S46: Absorption and emission spectra of complex **C11**.

Ligand L12

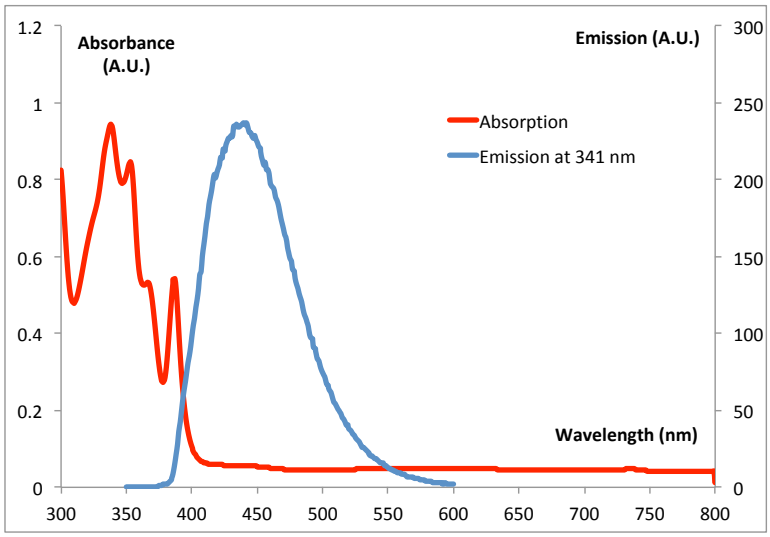

Quantum yield in DMSO at 298K: 61%
(Concentration: $3.3.10^{-5}$M)
UV-Vis (DMSO): λ_{max} (nm) (ε, $cm^{-1}.mol^{-1}.dm^3$) 338 (25928), 353 (24139), 366 (15420), 387 (15708).

Figure S47: Absorption and emission spectra of ligand **L12**.

Complex C12

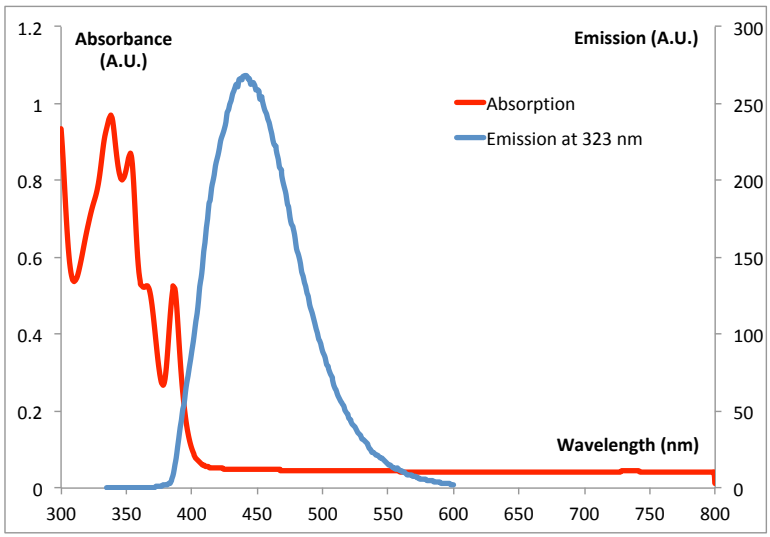

Quantum yield in DMSO at 298K: 71%

(Concentration: $2.2.10^{-5}$M)
UV-Vis (DMSO): λ_{max} (nm) (ε, $cm^{-1}.mol^{-1}.dm^3$) 338 (28904), 353 (28264), 366 (19892), 388 (20031).

Figure S48: Absorption and emission spectra of complex **C12**.

S3. Stability studies by UV-visible spectrophotometry

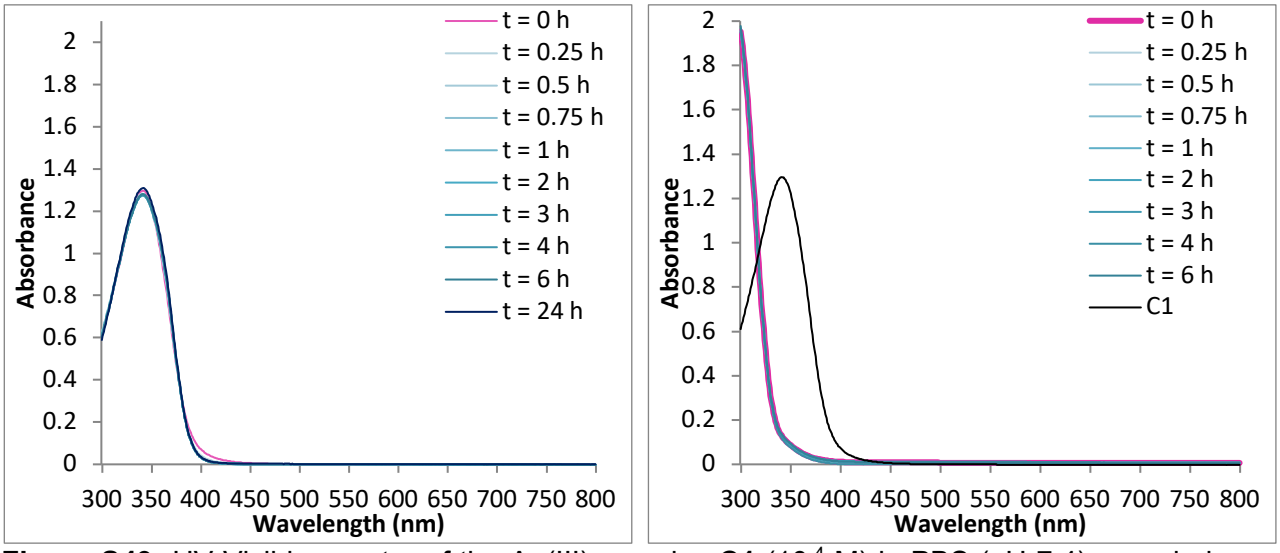

Figure S49: UV-Visible spectra of the Au(III) complex **C1** (10^{-4} M) in PBS (pH 7.4) recorded over time (left); and of **C1** before and after addition of GSH (2 eq.) recorded over time at room temperature (right).

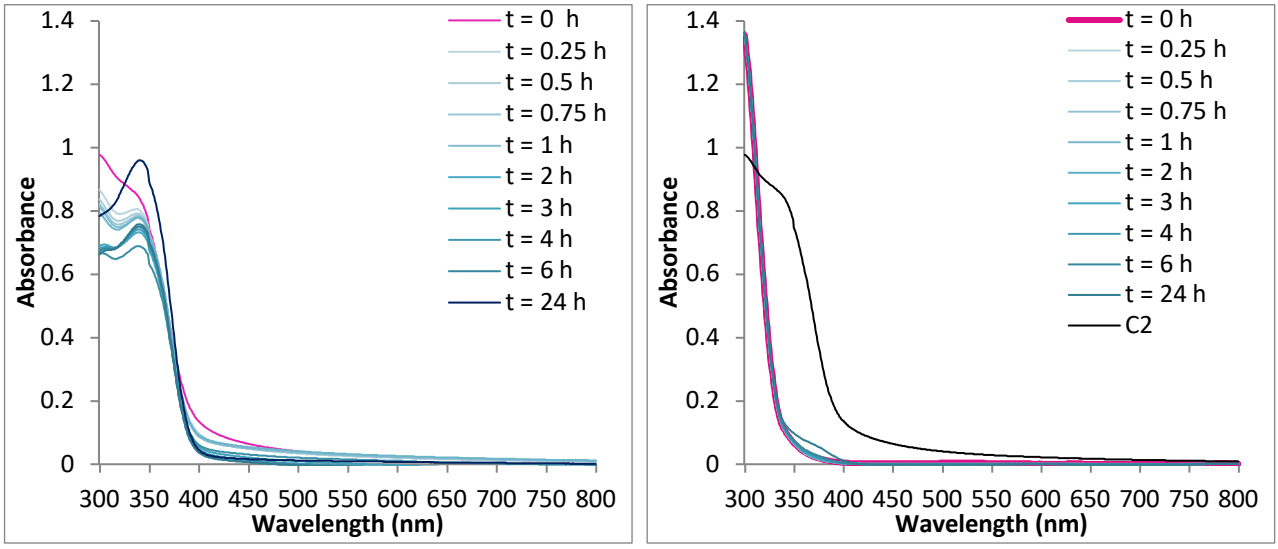

Figure S50: UV-Visible spectra of the Au(III) complex **C2** (10^{-4} M) in PBS (pH 7.4) recorded over time (left); and of **C2** before and after addition of GSH (2 eq.) recorded over time at room temperature (right).

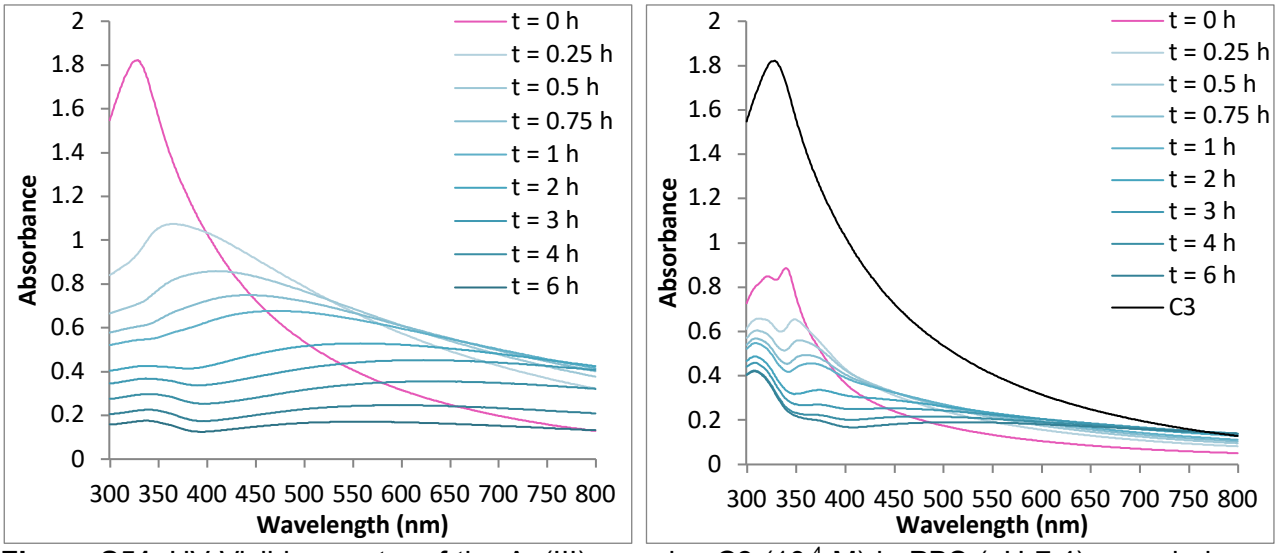

Figure S51: UV-Visible spectra of the Au(III) complex **C3** (10^{-4} M) in PBS (pH 7.4) recorded over time (left); and of **C3** before and after addition of GSH (2 eq.) recorded over time at room temperature (right).

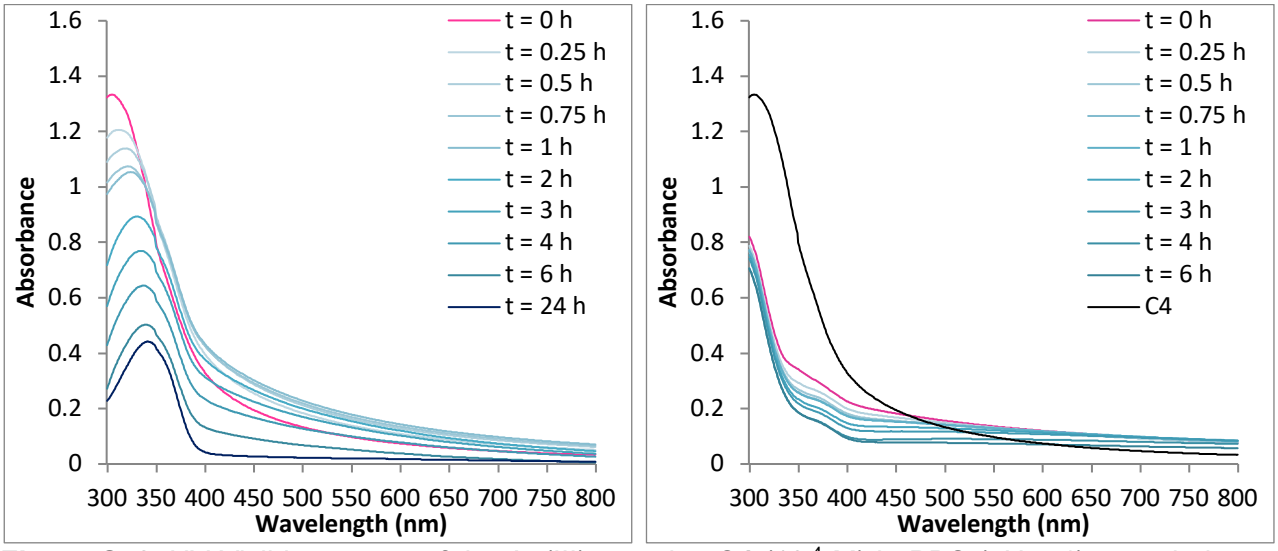

Figure S52: UV-Visible spectra of the Au(III) complex **C4** (10^{-4} M) in PBS (pH 7.4) recorded over time (left); and of **C4** before and after addition of GSH (2 eq.) recorded over time at room temperature (right).

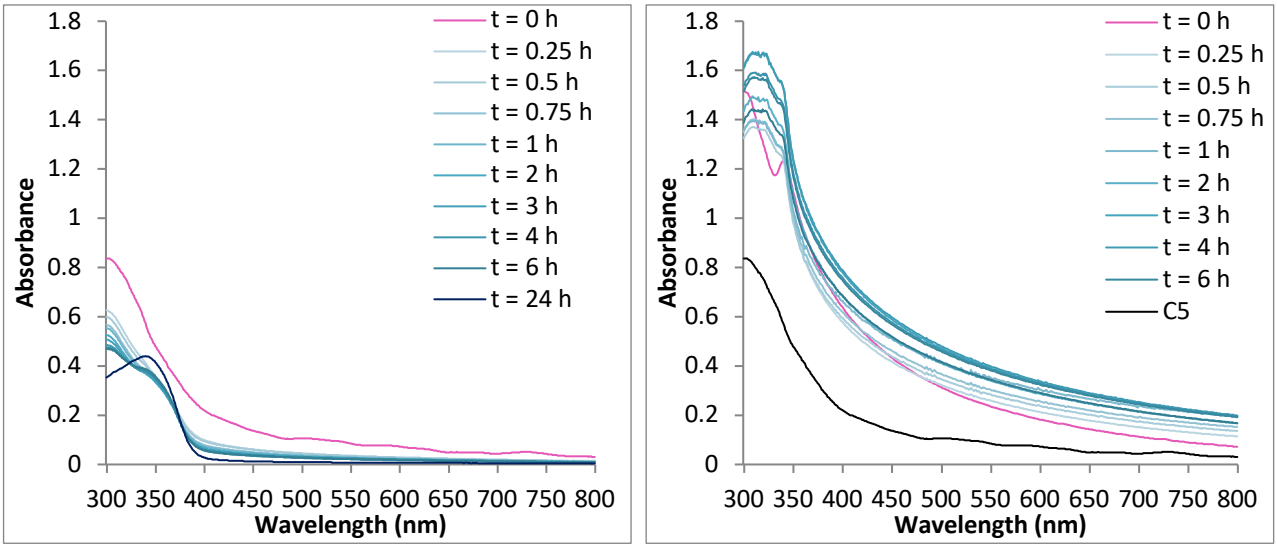

Figure S53: UV-Visible spectra of the Au(III) complex **C5** (10^{-4} M) in PBS (pH 7.4) recorded over time (left); and of **C5** before and after addition of GSH (2 eq.) recorded over time at room temperature (right).

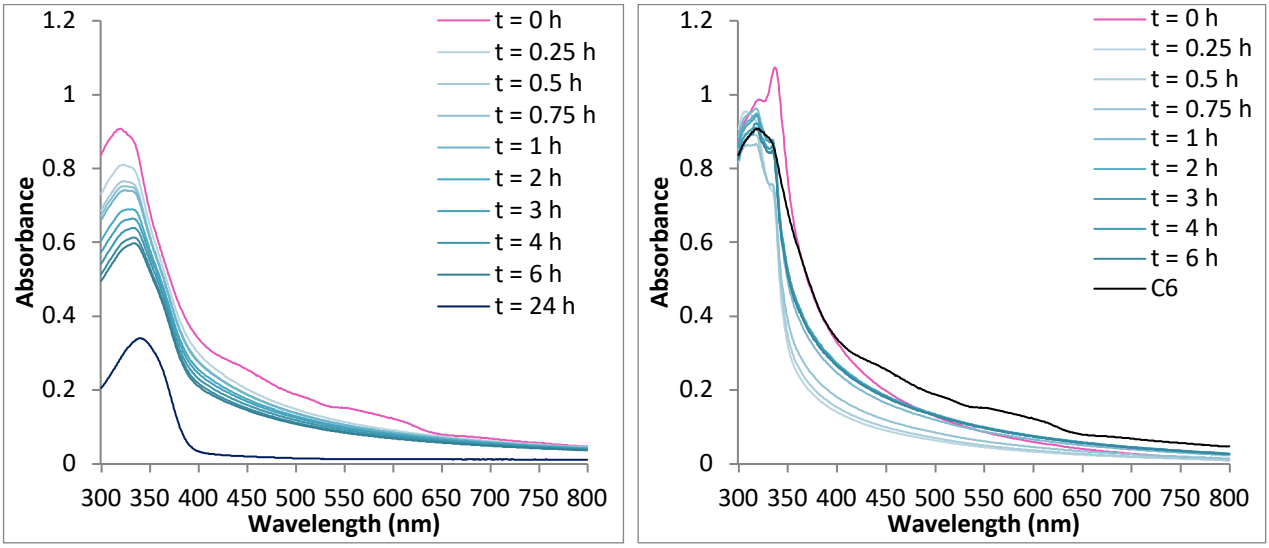

Figure S54: UV-Visible spectra of the Au(III) complex **C6** (10^{-4} M) in PBS (pH 7.4) recorded over time (left); and of **C6** before and after addition of GSH (2 eq.) recorded over time at room temperature (right).

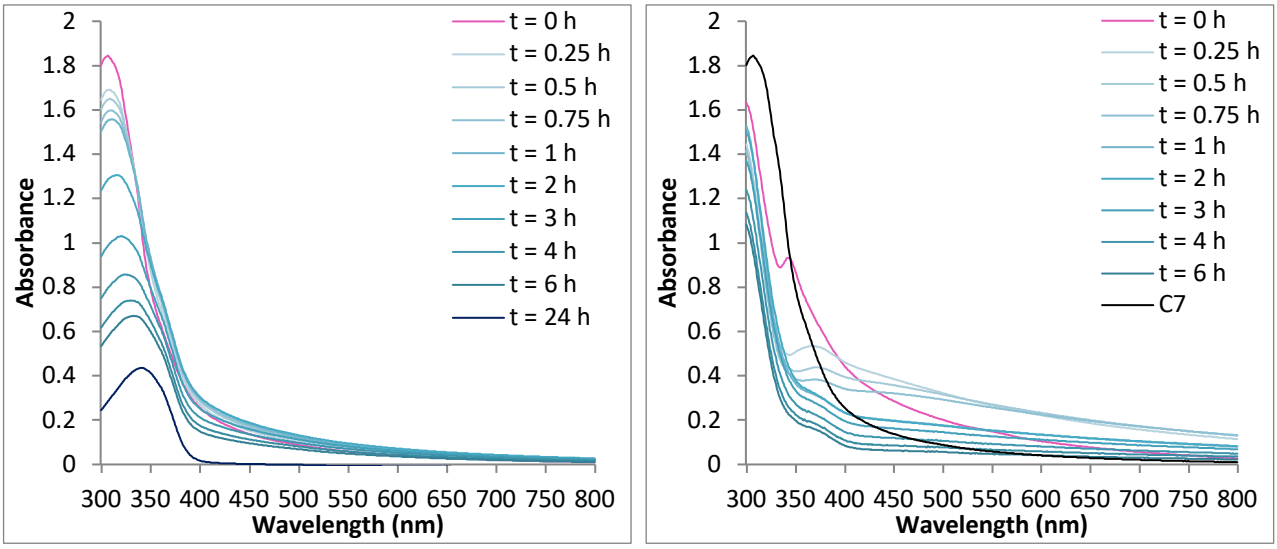

Figure S55: UV-Visible spectra of the Au(III) complex **C7** (10^{-4} M) in PBS (pH 7.4) recorded over time (left); and of **C7** before and after addition of GSH (2 eq.) recorded over time at room temperature (right).

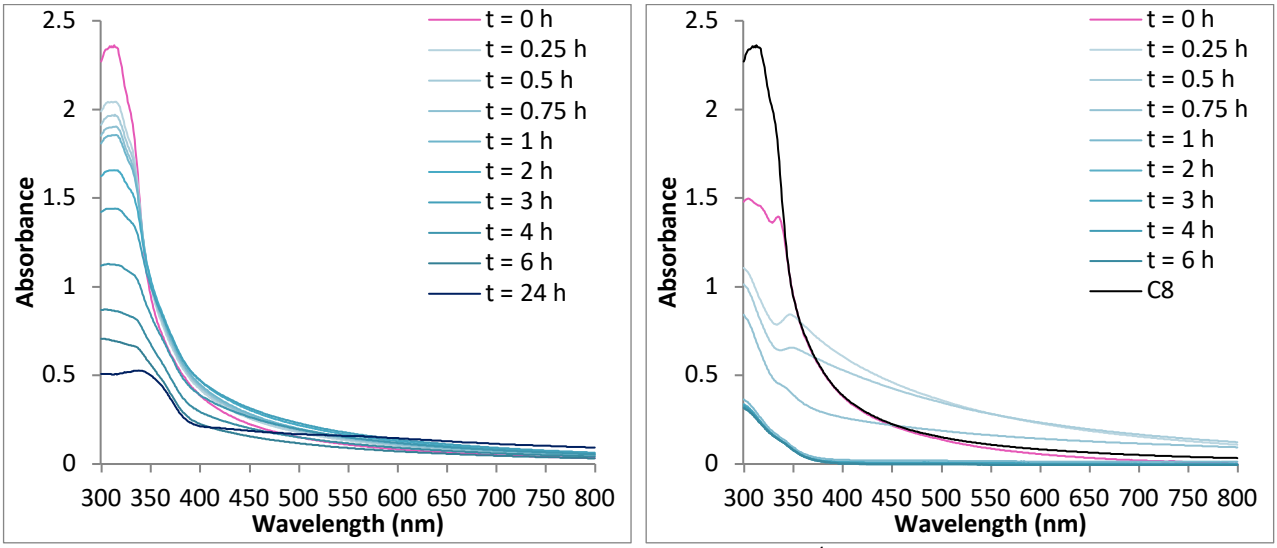

Figure S56: UV-Visible spectra of the Au(III) complex **C8** (10^{-4} M) in PBS (pH 7.4) recorded over time (left); and of **C8** before and after addition of GSH (2 eq.) recorded over time at room temperature (right).

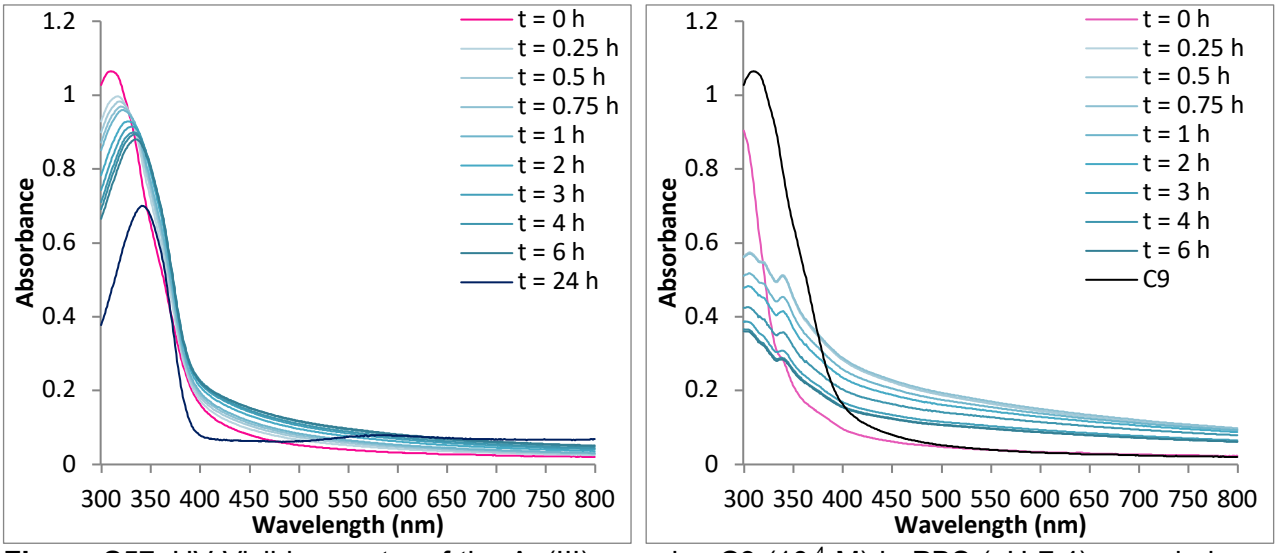

Figure S57: UV-Visible spectra of the Au(III) complex **C9** (10^{-4} M) in PBS (pH 7.4) recorded over time (left); and of **C9** before and after addition of GSH (2 eq.) recorded over time at room temperature (right).

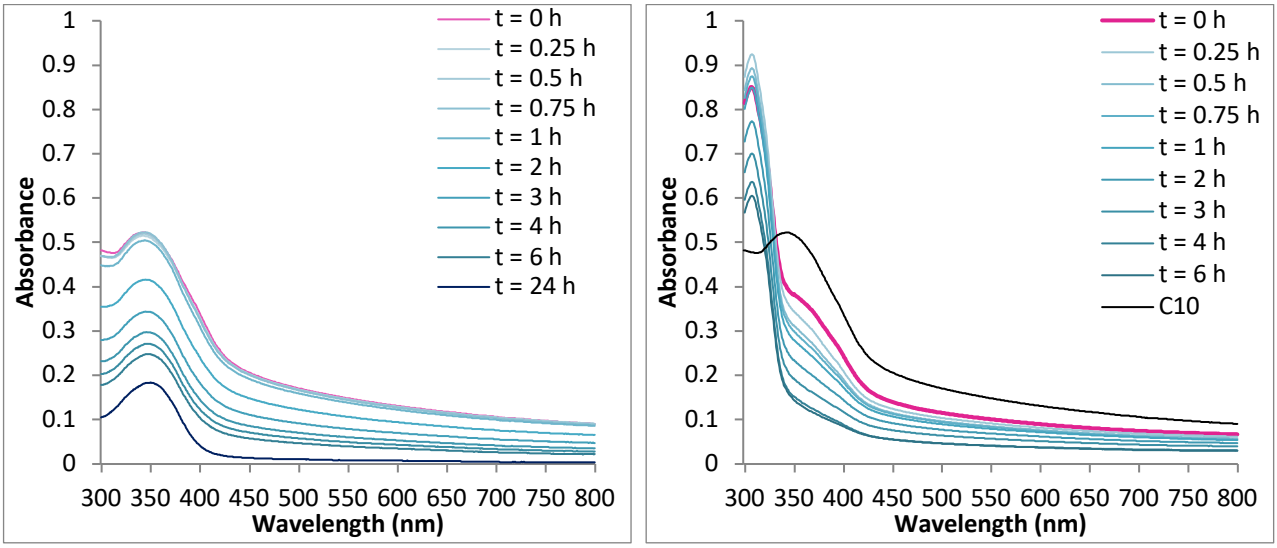

Figure S58: UV-Visible spectra of the Au(III) complex **C10** (10^{-4} M) in PBS (pH 7.4) recorded over time (left); and of **C10** before and after addition of GSH (2 eq.) recorded over time at room temperature (right).

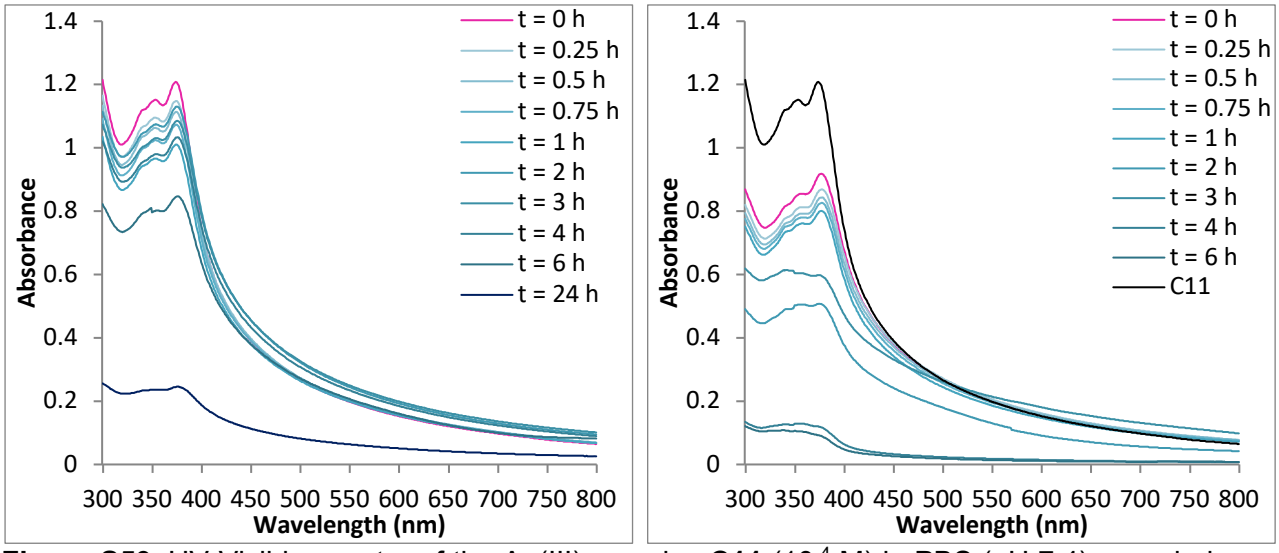

Figure S59: UV-Visible spectra of the Au(III) complex **C11** (10^{-4} M) in PBS (pH 7.4) recorded over time (left); and of **C11** before and after addition of GSH (2 eq.) recorded over time at room temperature (right).

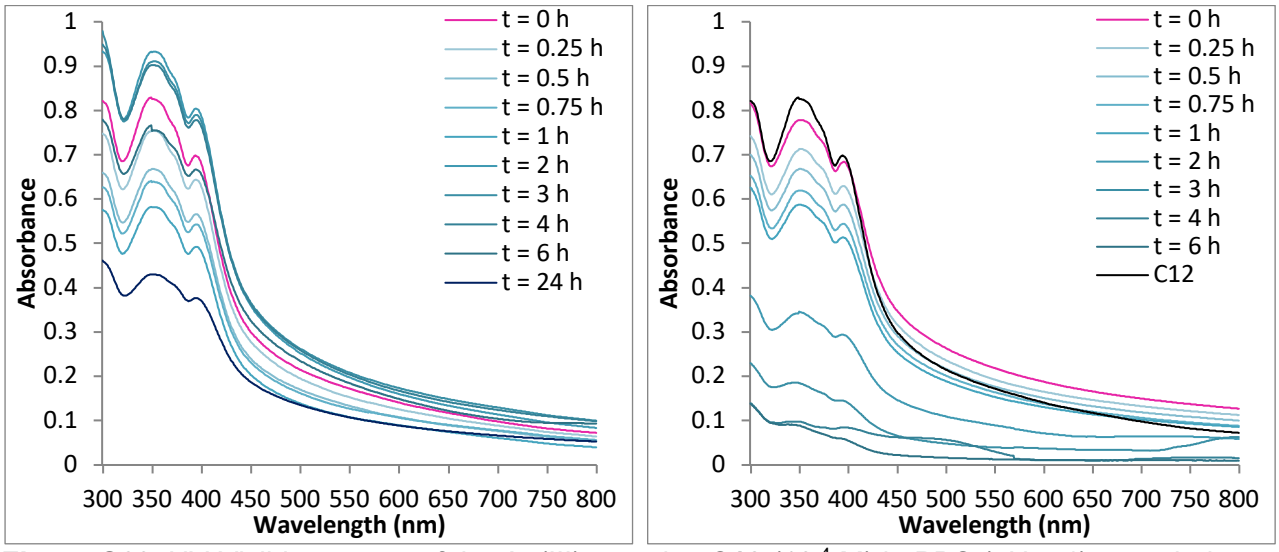

Figure S60: UV-Visible spectra of the Au(III) complex **C12** (10^{-4} M) in PBS (pH 7.4) recorded over time (left); and of **C12** before and after addition of GSH (2 eq.) recorded over time at room temperature (right).

Table S1. Antiproliferative activities (EC_{50} values) of ligands in human SKOV-3, A375, MCF-7, and A549 cells after 72 h incubation.

Compound	EC_{50} [μM] [1]			
	SKOV-3 (++)	A375 (+)	MCF7 (++)	A549 (+)
L1	>80	>80	>80	>80
L2	>80	n.d.	>80	>80
L3	38 ± 12	18 ± 2	44 ± 1	44 ± 3
L4	45 ± 3	53 ± 4	55 ± 3	61 ± 5
L5	>80 (n=1)	>80 (n=1)	31 (n=1)	>80 (n=1)
L6	36 (n=1)	26 ± 3	38 (n=1)	36 (n=2)
L7	>80 (n=1)	59 (n=1)	73 (n=1)	>80 (n=1)
L8	>80 (n=1)	>80 (n=1)	>80 (n=1)	>80 (n=1)
L9	60 (n=1)	45 (n=1)	55 (n=1)	54 (n=1)
L10	>80	>80	>80	>80
L11	>80	20 ± 2	4 ± 1	>80
L12	52 ± 21	17 (n=1)	23 ± 2	73 ± 8

[1] Values represented as mean (± SEM) of at least three independent experiments (n), unless otherwise stated. n.d.= non determined.

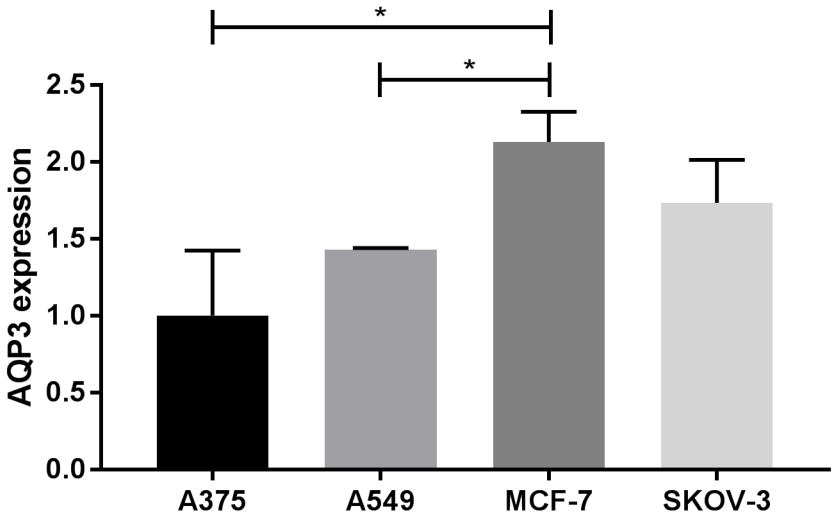

Figure S61. Normalized mean fluorescence intensity (MFI) of AQP3, detected using a secondary Alexa Fluor®488-labelled antibody. Results were normalized for the sample with the lowest expression (A375) and results are expressed as mean ± SEM of three independent experiments. *$p < 0.03$.

Submitted by: **Prof Casini**

Solved by: **Wim T Klooster**

Sample ID: **C6**

Crystal Data and Experimental

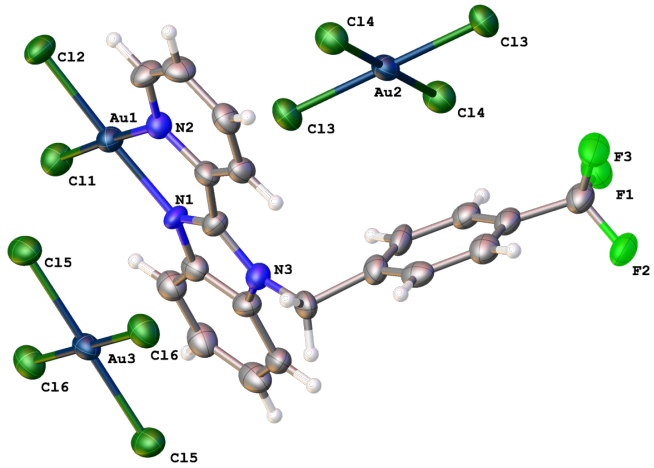

Figure S62: Thermal ellipsoids drawn at the 50% probability level.

Experimental. A suitable yellow block-shaped crystals of **2018ncs0304** (0.050×0.040×0.030) mm^3 was selected and mounted on a MITIGEN holder in perfluoroether oil on a Rigaku 007HF diffractometer equipped with Varimax confocal mirrors and an AFC11 goniometer and HyPix 6000HE detector. The crystal was kept at T = 100.00(10) K during data collection. Using **Olex2** (Dolomanov et al., 2009), the structure was solved with the **ShelXT** (Sheldrick, 2015) structure solution program, using the Intrinsic Phasing solution method. The model was refined with version 2014/7 of **ShelXL** (Sheldrick, 2015) using Least Squares minimisation.

Crystal Data. $C_{20}H_{14}Au_2Cl_6F_3N_3$, M_r = 959.97, triclinic, P-1 (No. 2), a = 9.1341(3) Å, b = 9.2310(3) Å, c = 16.4226(5) Å, α = 78.730(3)°, β = 86.795(2)°, γ = 71.093(3)°, V = 1284.69(8) Å^3, T = 100(2) K, Z = 2, Z' = 1, μ(CuK$_\alpha$) = 27.253 mm^{-1}, 23132 reflections measured, 4640 unique (R_{int} = 0.0720) which were used in all calculations. The final wR_2 was 0.1431 (all data) and R_1 was 0.0504 (I > 2(I)).

Compound	**2018ncs0304**
Formula	$C_{20}H_{14}Au_2Cl_6F_3N_3$
$D_{calc.}$/ g cm^{-3}	2.482
μ/mm^{-1}	27.253
Formula Weight	959.97
Colour	yellow
Shape	block
Size/mm^3	0.050×0.040×0.030
T/K	100(2)
Crystal System	triclinic
Space Group	P-1
a/Å	9.1341(3)
b/Å	9.2310(3)
c/Å	16.4226(5)
α/°	78.730(3)
β/°	86.795(2)
γ/°	71.093(3)
V/Å^3	1284.69(8)
Z	2
Z'	1
Wavelength/Å	1.54184
Radiation type	CuK$_\alpha$
Θ_{min}/°	2.744
Θ_{max}/°	68.244
Measured Refl.	23132
Independent Refl.	4640
Reflections Used	4211
R_{int}	0.0720
Parameters	310
Restraints	0
Largest Peak	3.059
Deepest Hole	-2.835
GooF	1.058
wR_2 (all data)	0.1431
wR_2	0.1400
R_1 (all data)	0.0543
R_1	0.0504

Structure Quality Indicators

Reflections:	d min (Cu) 0.83	I/σ 24.5	Rint 7.20%	complete 99% (IUCr) 99%
Refinement:	Shift -0.001	Max Peak 3.1	Min Peak -2.8	GooF 1.058

A yellow block-shaped crystal with dimensions 0.050×0.040×0.030 mm^3 was mounted on a MITIGEN holder in perfluoroether oil. X-ray diffraction data were collected using a Rigaku 007HF diffractometer equipped with Varimax confocal mirrors and an AFC11 goniometer and HyPix 6000HE detector, and equipped with an Oxford Cryosystems low-temperature device, operating at T = 100.00(10) K.

Data were measured using ω scans of 0.5 ° per frame for 0.5 s using CuK_α radiation (Rotating-anode X-ray tube, 40 kV, 30 mA). The total number of runs and images was based on the strategy calculation from the program **CrysAlisPro** (Rigaku, V1.171.39.46, 2018).The maximum resolution achieved was Θ = 68.244°.

Cell parameters were retrieved using the **CrysAlisPro** (Rigaku, V1.171.39.46, 2018) software and refined using **CrysAlisPro** (Rigaku, V1.171.39.46, 2018) on 10414 reflections, 45 % of the observed reflections.

Data reduction was performed using the **CrysAlisPro** (Rigaku, V1.171.39.46, 2018) software which corrects for Lorentz polarisation. The final completeness is 99.20 % out to 68.244° in Θ.

A multi-scan absorption correction was performed using CrysAlisPro 1.171.39.46 (Rigaku Oxford Diffraction, 2018) Empirical absorption correction using spherical harmonics, implemented in SCALE3 ABSPACK scaling algorithm. The absorption coefficient μ of this material is 27.253 mm^{-1} at this wavelength (λ = 1.54184Å) and the minimum and maximum transmissions are 0.12468 and 1.00000.

The structure was solved in the space group P-1 (# 2) by Intrinsic Phasing using the **ShelXT** (Sheldrick, 2015) structure solution program and refined by Least Squares using version 2014/7 of **ShelXL** (Sheldrick, 2015). All non-hydrogen atoms were refined anisotropically. Hydrogen atom positions were calculated geometrically and refined using the riding model.

There is a single molecule in the asymmetric unit, which is represented by the reported sum formula. In other words: Z is 2 and Z' is 1.

There is also an $AuCl_4^-$ molecule present, with two Au atoms at special positions.

There is room for a small solvent molecule, which could possibly be a (partial) MeOH, but could not be refined as such. The structure has been SQUEEZEd instead.

Reflection Statistics

Total reflections (after filtering)	23132	Unique reflections	4640
Completeness	0.991	Mean I/σ	18.3
hkl_{max} collected	(10, 10, 19)	hkl_{min} collected	(-10, -10, -19)
hkl_{max} used	(10, 10, 19)	hkl_{min} used	(-10, -10, 0)
Lim d_{max} collected	100.0	Lim d_{min} collected	0.77
d_{max} used	16.11	d_{min} used	0.83
Friedel pairs	2655	Friedel pairs merged	1
Inconsistent equivalents	2	R_{int}	0.072
R_{sigma}	0.0409	Intensity transformed	0
Omitted reflections	0	Omitted by user (OMIT hkl)	0
Multiplicity	(1548, 1951, 1350, 868, 538, 414, 305, 161, 74, 61, 13, 12)	Maximum multiplicity	16
Removed systematic absences	0	Filtered off (Shel/OMIT)	0

Table 1: Fractional Atomic Coordinates (×10⁴) and Equivalent Isotropic Displacement Parameters (Å²×10³) for **2018ncs0304**. U_{eq} is defined as 1/3 of the trace of the orthogonalised U_{ij}.

Atom	x	y	z	U_{eq}
Au01	5000	5000	5000	32.18(17)
Au02	2037.3(4)	7104.8(4)	7836.5(2)	31.28(16)
Au03	5000	5000	10000	35.20(18)
Cl04	3566(3)	4849(3)	6181.0(13)	40.9(5)
Cl05	6992(3)	5863(3)	9468.3(14)	45.2(5)
Cl06	5232(3)	7292(2)	5208.3(13)	42.2(5)
Cl07	195(3)	9452(3)	7553.4(15)	43.3(5)
Cl08	3284(3)	7423(3)	9598.5(15)	46.6(5)
Cl09	154(3)	6131(3)	8378.5(15)	42.5(5)
F00A	11945(6)	870(6)	4901(4)	46.0(13)
F00B	9696(7)	1494(7)	4337(3)	51.1(13)
F00C	10868(7)	3197(6)	4224(4)	53.4(15)
N00D	3821(8)	5114(7)	8048(4)	29.6(14)
N00E	6361(8)	3909(8)	7985(4)	32.7(15)
N00F	3801(8)	7908(8)	7377(4)	31.4(14)
C00G	5207(9)	5273(9)	7833(5)	30.4(16)
C00H	3632(11)	9404(9)	7021(6)	37.4(19)
C00I	4058(10)	3538(9)	8343(5)	32.3(17)
C00J	5270(10)	6827(9)	7460(5)	31.6(17)
C00K	8412(10)	2324(9)	5781(5)	34.3(18)
C00L	6364(11)	8811(10)	6863(5)	36.1(18)
C00M	6297(11)	1151(10)	8557(5)	36.6(19)
C00N	10589(11)	2015(10)	4754(6)	40(2)
C00O	9848(10)	2494(9)	5543(5)	35.6(18)
C00P	8018(11)	3538(10)	7911(5)	36.1(19)
C00Q	8570(11)	3260(9)	7030(6)	35.4(18)
C00R	5632(11)	2781(9)	8292(5)	35.9(18)
C00S	10644(12)	3072(10)	6016(6)	40(2)
C00T	3053(12)	2711(10)	8652(5)	39.4(19)
C00U	10016(11)	3461(9)	6780(6)	37(2)
C00V	4880(11)	9889(10)	6760(5)	40(2)
C00W	7825(10)	2728(9)	6517(6)	36.7(19)
C00X	5306(13)	363(10)	8856(6)	45(2)
C00Y	6541(10)	7261(10)	7196(5)	32.4(17)
C00Z	3678(12)	1118(10)	8900(5)	44(2)

Table 2: Anisotropic Displacement Parameters (×10⁴) **2018ncs0304**. The anisotropic displacement factor exponent takes the form: $-2\pi^2[h^2a^{*2} \times U_{11} + ... + 2hka^* \times b^* \times U_{12}]$

Atom	U_{11}	U_{22}	U_{33}	U_{23}	U_{13}	U_{12}
Au01	38.1(3)	31.2(3)	26.9(3)	-2.84(19)	0.0(2)	-12.0(2)
Au02	32.5(2)	26.6(2)	31.6(2)	-2.73(15)	0.82(15)	-6.98(16)
Au03	50.2(3)	28.1(3)	26.6(3)	-3.45(19)	1.5(2)	-12.7(2)
Cl04	46.7(12)	48.6(12)	30.6(10)	-8.4(8)	6.0(8)	-20.0(10)
Cl05	59.6(15)	42.3(12)	38.1(11)	-9.0(9)	6.4(10)	-22.5(11)
Cl06	53.2(13)	37.2(10)	40.2(11)	-7.1(8)	0.7(9)	-20.0(9)
Cl07	36.8(11)	31.3(11)	51.3(13)	-0.9(9)	2.8(9)	-1.1(8)
Cl08	61.7(15)	30.7(10)	42.7(12)	-4.9(9)	-5.0(10)	-8.9(10)
Cl09	39.0(12)	39.2(11)	49.7(12)	-6.2(9)	4.4(9)	-15.1(9)
F00A	40(3)	33(3)	53(3)	-5(2)	13(2)	0(2)
F00B	64(4)	49(3)	40(3)	-10(2)	9(3)	-17(3)
F00C	63(4)	36(3)	50(3)	4(2)	22(3)	-11(3)
N00D	26(3)	21(3)	32(3)	1(3)	4(3)	2(3)
N00E	34(4)	26(3)	32(4)	-4(3)	6(3)	-4(3)
N00F	33(4)	28(3)	30(3)	-4(3)	4(3)	-8(3)
C00G	31(4)	25(4)	31(4)	-6(3)	-2(3)	-4(3)
C00H	38(5)	20(4)	47(5)	0(3)	-1(4)	-4(3)
C00I	45(5)	25(4)	28(4)	-6(3)	0(3)	-11(3)
C00J	42(5)	26(4)	24(4)	-2(3)	4(3)	-9(3)
C00K	35(4)	24(4)	40(4)	-5(3)	-3(4)	-4(3)
C00L	44(5)	38(4)	31(4)	-7(3)	8(4)	-20(4)
C00M	45(5)	29(4)	28(4)	-6(3)	0(4)	-2(4)
C00N	44(5)	27(4)	45(5)	-5(4)	7(4)	-6(4)
C00O	37(5)	22(4)	39(5)	-1(3)	7(4)	-2(3)
C00P	49(5)	31(4)	25(4)	-11(3)	4(4)	-5(4)
C00Q	41(5)	25(4)	37(4)	-9(3)	8(4)	-6(4)
C00R	46(5)	25(4)	31(4)	-1(3)	-1(4)	-6(4)
C00S	44(5)	27(4)	45(5)	-2(4)	6(4)	-10(4)
C00T	50(5)	33(4)	36(4)	-6(3)	4(4)	-15(4)
C00U	46(5)	21(4)	41(5)	-4(3)	-9(4)	-8(4)
C00V	54(6)	27(4)	35(5)	6(3)	-1(4)	-15(4)
C00W	35(5)	23(4)	44(5)	-5(3)	18(4)	-3(3)
C00X	72(7)	29(4)	35(4)	-5(3)	2(4)	-18(4)
C00Y	30(4)	35(4)	29(4)	-1(3)	2(3)	-10(3)
C00Z	62(7)	35(5)	40(5)	-9(4)	12(5)	-23(5)

Table 3: Bond Lengths in Å for **2018ncs0304**.

Atom	Atom	Length/Å
Au01	Cl04	2.286(2)
Au01	Cl04[1]	2.286(2)
Au01	Cl06[1]	2.285(2)
Au01	Cl06	2.285(2)
Au02	Cl07	2.252(2)
Au02	Cl09	2.253(2)
Au02	N00D	2.006(6)
Au02	N00F	2.034(7)
Au03	Cl05	2.279(2)
Au03	Cl05[2]	2.279(2)
Au03	Cl08	2.272(2)
Au03	Cl08[2]	2.272(2)
F00A	C00N	1.340(10)
F00B	C00N	1.347(11)
F00C	C00N	1.340(10)
N00D	C00G	1.342(11)
N00D	C00I	1.389(10)
N00E	C00G	1.344(10)
N00E	C00P	1.444(12)
N00E	C00R	1.409(11)
N00F	C00H	1.352(11)
N00F	C00J	1.383(11)
C00G	C00J	1.463(11)
C00H	C00V	1.372(13)
C00I	C00R	1.386(13)
C00I	C00T	1.391(12)
C00J	C00Y	1.370(12)
C00K	C00O	1.397(12)
C00K	C00W	1.365(12)
C00L	C00V	1.394(13)
C00L	C00Y	1.388(12)
C00M	C00R	1.416(11)
C00M	C00X	1.353(14)
C00N	C00O	1.505(12)
C00O	C00S	1.376(13)
C00P	C00Q	1.546(11)
C00Q	C00U	1.420(13)
C00Q	C00W	1.363(13)
C00S	C00U	1.412(13)
C00T	C00Z	1.379(12)
C00X	C00Z	1.427(14)

[1]1-x,1-y,1-z; [2]1-x,1-y,2-z

Table 4: Bond Angles in ° for **2018ncs0304**.

Atom	Atom	Atom	Angle/°
Cl04	Au01	Cl04[1]	180.0
Cl06[1]	Au01	Cl04[1]	90.30(8)
Cl06[1]	Au01	Cl04	89.70(8)
Cl06	Au01	Cl04	90.30(8)
Cl06	Au01	Cl04[1]	89.71(8)
Cl06	Au01	Cl06[1]	180.0
Cl07	Au02	Cl09	87.34(9)
N00D	Au02	Cl07	174.7(2)
N00D	Au02	Cl09	97.9(2)
N00D	Au02	N00F	79.9(3)
N00F	Au02	Cl07	94.8(2)
N00F	Au02	Cl09	177.6(2)
Cl05	Au03	Cl05[2]	180.0
Cl08	Au03	Cl05	90.62(9)
Cl08[2]	Au03	Cl05	89.38(9)
Cl08[2]	Au03	Cl05[2]	90.62(9)
Cl08	Au03	Cl05[2]	89.38(9)
Cl08[2]	Au03	Cl08	180.00(13)
C00G	N00D	Au02	114.7(5)
C00G	N00D	C00I	107.2(6)
C00I	N00D	Au02	138.1(6)
C00G	N00E	C00P	131.6(7)
C00G	N00E	C00R	105.2(7)
C00R	N00E	C00P	123.1(7)
C00H	N00F	Au02	124.7(6)
C00H	N00F	C00J	119.1(7)
C00J	N00F	Au02	116.2(5)
N00D	C00G	N00E	112.4(7)
N00D	C00G	C00J	118.2(7)
N00E	C00G	C00J	129.4(8)
N00F	C00H	C00V	121.8(8)
N00D	C00I	C00T	132.3(8)
C00R	C00I	N00D	106.8(7)
C00R	C00I	C00T	120.9(8)
N00F	C00J	C00G	110.9(7)
C00Y	C00J	N00F	120.7(7)
C00Y	C00J	C00G	128.3(8)
C00W	C00K	C00O	117.4(8)
C00Y	C00L	C00V	119.2(8)
C00X	C00M	C00R	116.2(9)
F00A	C00N	F00B	106.8(7)
F00A	C00N	F00C	106.9(7)
F00A	C00N	C00O	111.8(8)
F00B	C00N	C00O	112.4(8)
F00C	C00N	F00B	106.1(8)
F00C	C00N	C00O	112.4(7)
C00K	C00O	C00N	120.2(8)
C00S	C00O	C00K	122.1(8)
C00S	C00O	C00N	117.7(8)
N00E	C00P	C00Q	111.6(7)
C00U	C00Q	C00P	116.6(8)
C00W	C00Q	C00P	124.4(8)
C00W	C00Q	C00U	118.8(8)
N00E	C00R	C00M	129.3(8)
C00I	C00R	N00E	108.3(7)
C00I	C00R	C00M	122.3(8)
C00O	C00S	C00U	119.2(9)
C00Z	C00T	C00I	117.6(9)
C00S	C00U	C00Q	118.7(8)
C00H	C00V	C00L	119.2(8)
C00Q	C00W	C00K	123.7(8)
C00M	C00X	C00Z	122.3(8)
C00J	C00Y	C00L	119.8(8)
C00T	C00Z	C00X	120.7(9)

[1]1-x,1-y,1-z; [2]1-x,1-y,2-z

Table 5: Torsion Angles in ° for **2018ncs0304**.

Atom	Atom	Atom	Atom	Angle/°
Au02	N00D	C00G	N00E	-179.9(5)
Au02	N00D	C00G	C00J	-1.4(9)
Au02	N00D	C00I	C00R	177.6(6)
Au02	N00D	C00I	C00T	-2.8(15)
Au02	N00F	C00H	C00V	176.6(7)
Au02	N00F	C00J	C00G	3.2(8)
Au02	N00F	C00J	C00Y	-177.8(6)
F00A	C00N	C00O	C00K	-118.1(8)
F00A	C00N	C00O	C00S	60.9(10)
F00B	C00N	C00O	C00K	2.0(11)
F00B	C00N	C00O	C00S	-179.0(7)
F00C	C00N	C00O	C00K	121.6(9)
F00C	C00N	C00O	C00S	-59.4(11)
N00D	C00G	C00J	N00F	-1.2(10)
N00D	C00G	C00J	C00Y	179.9(8)
N00D	C00I	C00R	N00E	1.6(9)
N00D	C00I	C00R	C00M	178.9(7)
N00D	C00I	C00T	C00Z	-179.9(8)
N00E	C00G	C00J	N00F	176.9(8)
N00E	C00G	C00J	C00Y	-1.9(14)
N00E	C00P	C00Q	C00U	157.3(7)
N00E	C00P	C00Q	C00W	-27.9(11)
N00F	C00H	C00V	C00L	0.1(14)
N00F	C00J	C00Y	C00L	1.9(12)
C00G	N00D	C00I	C00R	-0.1(9)
C00G	N00D	C00I	C00T	179.5(9)
C00G	N00E	C00P	C00Q	-88.2(10)
C00G	N00E	C00R	C00I	-2.4(9)
C00G	N00E	C00R	C00M	-179.5(8)
C00G	C00J	C00Y	C00L	-179.3(8)
C00H	N00F	C00J	C00G	-178.2(7)
C00H	N00F	C00J	C00Y	0.8(12)
C00I	N00D	C00G	N00E	-1.6(9)
C00I	N00D	C00G	C00J	176.9(7)
C00I	C00T	C00Z	C00X	1.4(13)
C00J	N00F	C00H	C00V	-1.8(13)
C00K	C00O	C00S	C00U	2.1(12)
C00M	C00X	C00Z	C00T	-1.6(14)
C00N	C00O	C00S	C00U	-176.9(8)
C00O	C00K	C00W	C00Q	-1.0(12)
C00O	C00S	C00U	C00Q	-0.8(12)
C00P	N00E	C00G	N00D	-175.1(8)
C00P	N00E	C00G	C00J	6.7(14)
C00P	N00E	C00R	C00I	175.4(7)
C00P	N00E	C00R	C00M	-1.7(13)
C00P	C00Q	C00U	C00S	173.8(7)
C00P	C00Q	C00W	C00K	-172.5(8)
C00R	N00E	C00G	N00D	2.5(9)
C00R	N00E	C00G	C00J	-175.8(8)
C00R	N00E	C00P	C00Q	94.6(9)
C00R	C00I	C00T	C00Z	-0.3(12)
C00R	C00M	C00X	C00Z	0.5(13)
C00T	C00I	C00R	N00E	-178.1(7)
C00T	C00I	C00R	C00M	-0.7(13)
C00U	C00Q	C00W	C00K	2.2(13)
C00V	C00L	C00Y	C00J	-3.6(13)
C00W	C00K	C00O	C00N	177.7(8)
C00W	C00K	C00O	C00S	-1.2(12)

Atom	Atom	Atom	Atom	Angle/°
C00W	C00Q	C00U	C00S	-1.2(12)
C00X	C00M	C00R	N00E	177.3(9)
C00X	C00M	C00R	C00I	0.6(12)
C00Y	C00L	C00V	C00H	2.6(13)

Table 6: Hydrogen Fractional Atomic Coordinates ($\times 10^4$) and Equivalent Isotropic Displacement Parameters ($Å^2 \times 10^3$) for **2018ncs0304**. U_{eq} is defined as 1/3 of the trace of the orthogonalised U_{ij}.

Atom	x	y	z	U_{eq}
H00H	2621	10140	6949	45
H00K	7865	1943	5443	41
H00L	7244	9134	6708	43
H00M	7379	639	8525	44
H00A	8529	2590	8323	43
H00B	8327	4405	8036	43
H00S	11603	3209	5831	48
H00T	1973	3226	8691	47
H00U	10552	3848	7121	44
H00V	4733	10947	6513	48
H00W	6841	2632	6681	44
H00X	5707	-733	9045	54
H00Y	7542	6504	7241	39
H00Z	3019	518	9101	53

Table 7: Solvent masking (Olex2) information for **2018ncs0304**.

No	x	y	z	V	e	Content
1	0.000	0.000	0.000	87.7	6.0	?

Citations

CrysAlisPro Software System, Rigaku Oxford Diffraction, (2018).

O.V. Dolomanov and L.J. Bourhis and R.J. Gildea and J.A.K. Howard and H. Puschmann, Olex2: A complete structure solution, refinement and analysis program, *J. Appl. Cryst.*, (2009), **42**, 339-341.

Sheldrick, G.M., Crystal structure refinement with ShelXL, *Acta Cryst.*, (2015), **C27**, 3-8.

Sheldrick, G.M., ShelXT-Integrated space-group and crystal-structure determination, *Acta Cryst.*, (2015), **A71**, 3-8.

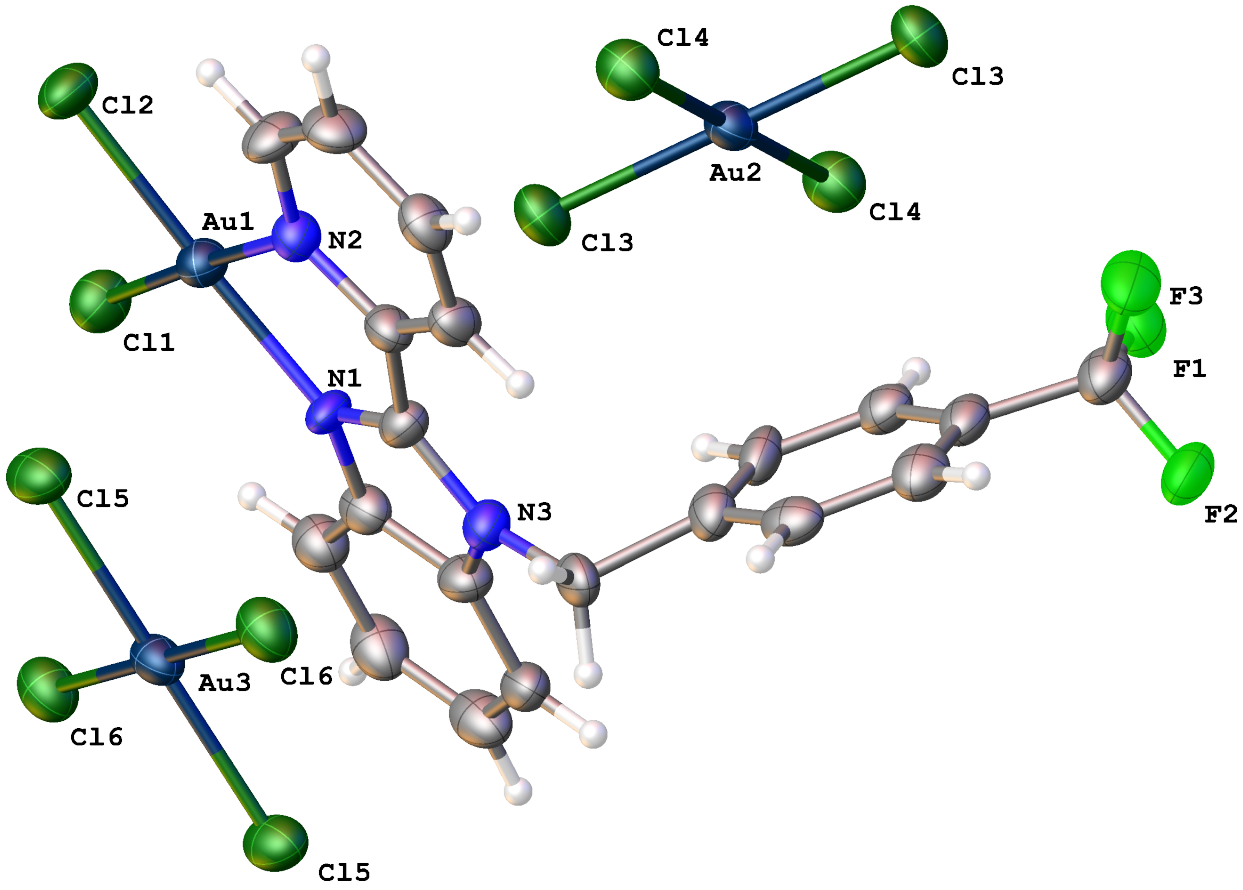
Cl4
Cl3
Au2
Cl4
Cl3
Cl2
Au1
N2
Cl1
N1
F3
F1
F2
Cl5
N3
Au3
Cl6
Cl6
Cl5

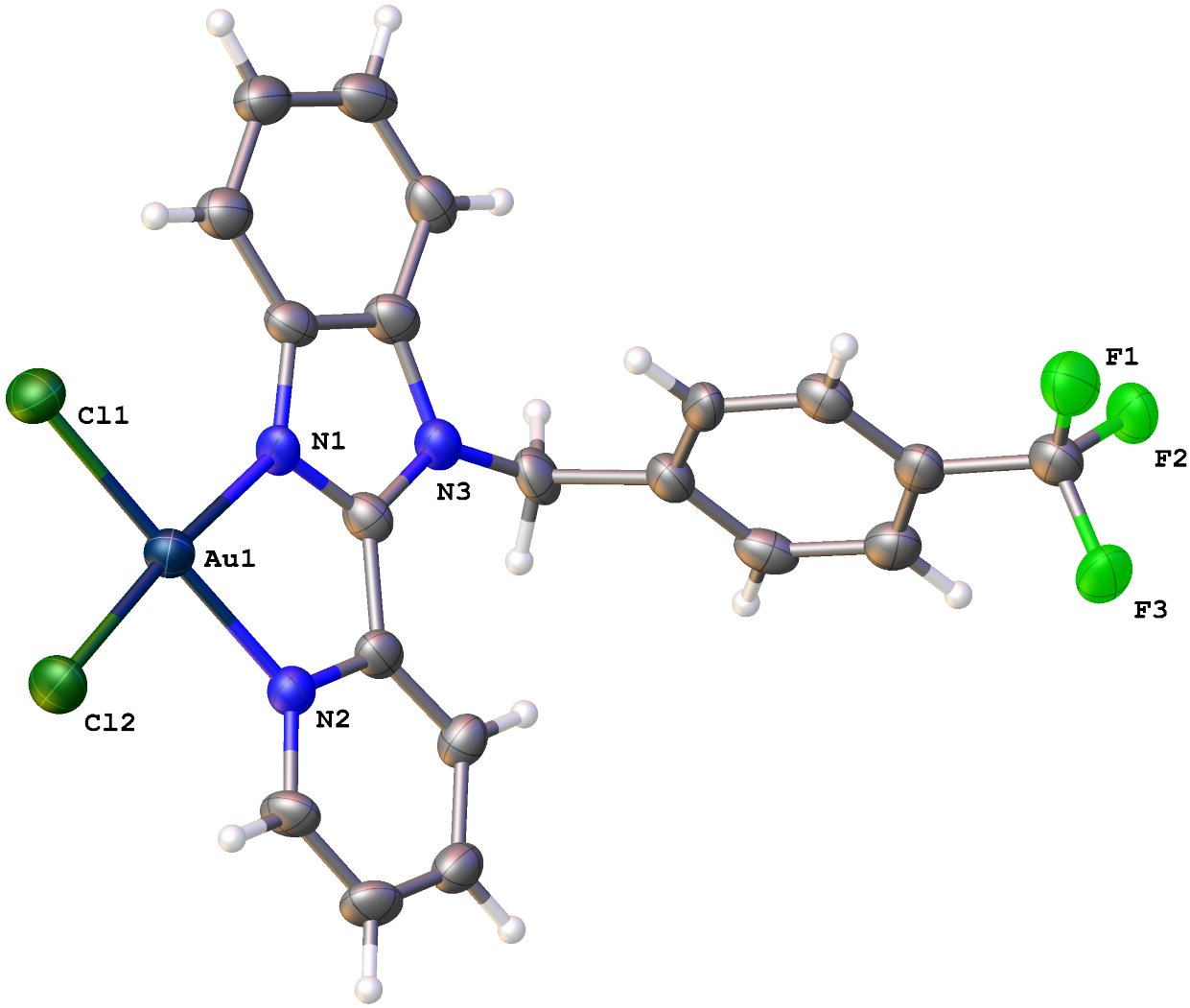
Cl1
N1
N3
F1
F2
Au1
F3
Cl2
N2

Submitted by: **Prof Casini**

Solved by: **Wim T Klooster**

Sample ID: **7**

Crystal Data and Experimental

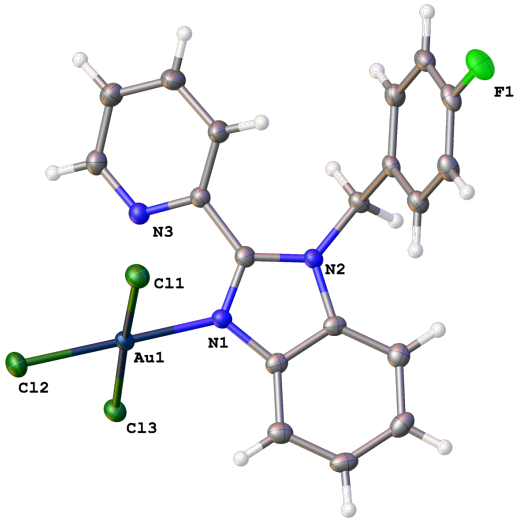

Figure S63: Thermal ellipsoids drawn at the 50% probability level.

Experimental. A suitable yellow plate-shaped crystal of **2018ncs0303** (0.080×0.050×0.020) mm³ was selected and mounted on a MITIGEN holder on a Rigaku 007HF diffractometer equipped with Varimax confocal mirrors and an AFC11 goniometer and HyPix 6000HE detector. The crystal was kept at T = 100.00(10) K during data collection. Using **Olex2** (Dolomanov et al., 2009), the structure was solved with the **ShelXT** (Sheldrick, 2015) structure solution program, using the Intrinsic Phasing solution method. The model was refined with version 2014/7 of **ShelXL** (Sheldrick, 2015) using Least Squares minimisation.

Crystal Data. $C_{19}H_{14}AuCl_3FN_3$, M_r = 606.65, monoclinic, $P2_1/n$ (No. 14), a = 12.19750(10) Å, b = 9.77810(10) Å, c = 17.08670(10) Å, β = 108.9480(10)°, α = γ = 90°, V = 1927.48(3) Å³, T = 100(2) K, Z = 4, Z' = 1, μ(CuK$_\alpha$) = 18.336 mm^{-1}, 34653 reflections measured, 3523 unique (R_{int} = 0.0329) which were used in all calculations. The final wR_2 was 0.0440 (all data) and R_1 was 0.0167 (I > 2(I)).

Compound	**2018ncs0303**
Formula	$C_{19}H_{14}AuCl_3FN_3$
$D_{calc.}$/ g cm^{-3}	2.091
μ/mm^{-1}	18.336
Formula Weight	606.65
Colour	yellow
Shape	plate
Size/mm³	0.080×0.050×0.020
T/K	100(2)
Crystal System	monoclinic
Space Group	$P2_1/n$
a/Å	12.19750(10)
b/Å	9.77810(10)
c/Å	17.08670(10)
α/°	90
β/°	108.9480(10)
γ/°	90
V/Å³	1927.48(3)
Z	4
Z'	1
Wavelength/Å	1.54184
Radiation type	CuK$_\alpha$
Θ_{min}/°	3.919
Θ_{max}/°	68.251
Measured Refl.	34653
Independent Refl.	3523
Reflections Used	3499
R_{int}	0.0329
Parameters	244
Restraints	0
Largest Peak	0.623
Deepest Hole	-0.726
GooF	1.086
wR_2 (all data)	0.0440
wR_2	0.0439
R_1 (all data)	0.0169
R_1	0.0167

Structure Quality Indicators

Reflections:	d min (Cu) 0.83	I/σ 70.0	Rint 3.29%	complete 100% (IUCr) 100%
Refinement:	Shift -0.003	Max Peak 0.6	Min Peak -0.7	GooF 1.086

A yellow plate-shaped crystal with dimensions 0.080×0.050×0.020 mm^3 was mounted on a MITIGEN holder. X-ray diffraction data were collected using a Rigaku 007HF diffractometer equipped with Varimax confocal mirrors and an AFC11 goniometer and HyPix 6000HE detector, and equipped with an Oxford Cryosystems low-temperature device, operating at T = 100.00(10) K.

Data were measured using ω scans of 0.5 ° per frame for 1.0 s using CuK_α radiation (Rotating-anode X-ray tube, 40 kV, 30 mA). The total number of runs and images was based on the strategy calculation from the program **CrysAlisPro** (Rigaku, V1.171.39.46, 2018). The maximum resolution achieved was Θ = 68.251°.

Cell parameters were retrieved using the **CrysAlisPro** (Rigaku, V1.171.39.46, 2018) software and refined using **CrysAlisPro** (Rigaku, V1.171.39.46, 2018) on 26320 reflections, 76 % of the observed reflections.

Data reduction was performed using the **CrysAlisPro** (Rigaku, V1.171.39.46, 2018) software which corrects for Lorentz polarisation. The final completeness is 99.90 % out to 68.251° in Θ.

A multi-scan absorption correction was performed using CrysAlisPro 1.171.39.46 (Rigaku Oxford Diffraction, 2018) Empirical absorption correction using spherical harmonics, implemented in SCALE3 ABSPACK scaling algorithm. The absorption coefficient μ of this material is 18.336 mm^{-1} at this wavelength (λ = 1.54184Å) and the minimum and maximum transmissions are 0.44132 and 1.00000.

The structure was solved in the space group $P2_1/n$ (# 14) by Intrinsic Phasing using the **ShelXT** (Sheldrick, 2015) structure solution program and refined by Least Squares using version 2014/7 of **ShelXL** (Sheldrick, 2015). All non-hydrogen atoms were refined anisotropically. Hydrogen atom positions were calculated geometrically and refined using the riding model.

There is a single molecule in the asymmetric unit, which is represented by the reported sum formula. In other words: Z is 4 and Z' is 1.

Reflection Statistics

Total reflections (after filtering)	35917	Unique reflections	3523
Completeness	0.999	Mean I/σ	54.85
hkl_{max} collected	(14, 11, 20)	hkl_{min} collected	(-14, -11, -20)
hkl_{max} used	(13, 11, 20)	hkl_{min} used	(-14, 0, 0)
Lim d_{max} collected	100.0	Lim d_{min} collected	0.77
d_{max} used	16.16	d_{min} used	0.83
Friedel pairs	4978	Friedel pairs merged	1
Inconsistent equivalents	0	R_{int}	0.0329
R_{sigma}	0.0143	Intensity transformed	0
Omitted reflections	0	Omitted by user (OMIT hkl)	0
Multiplicity	(2807, 3248, 2021, 1524, 1076, 592, 414, 170, 79, 51, 4)	Maximum multiplicity	26
Removed systematic absences	1264	Filtered off (Shel/OMIT)	0

Table 1: Fractional Atomic Coordinates (×10⁴) and Equivalent Isotropic Displacement Parameters (Å²×10³) for **2018ncs0303**. U_{eq} is defined as 1/3 of the trace of the orthogonalised U_{ij}.

Atom	x	y	z	U_{eq}
Au1	7564.7(2)	1459.3(2)	5627.6(2)	17.11(5)
Cl1	8834.0(6)	1625.2(7)	4903.3(4)	23.57(14)
Cl2	8494.3(6)	-466.6(6)	6241.8(4)	24.44(14)
Cl3	6216.1(6)	1236.9(7)	6290.3(4)	22.30(13)
F1	8554.0(16)	8147.3(18)	2035.5(11)	32.6(4)
N1	6755.9(19)	3168(2)	5055.3(13)	17.8(4)
N2	6494.9(18)	5305(2)	4616.4(12)	16.9(4)
N3	8589.4(19)	4009(2)	6452.0(13)	20.5(4)
C1	5657(2)	3243(3)	4465.4(15)	18.2(5)
C2	4822(2)	2245(3)	4147.2(16)	22.1(5)
C3	3807(2)	2665(3)	3554.6(16)	23.5(6)
C4	3629(2)	4027(3)	3290.2(16)	23.8(6)
C5	4461(2)	5029(3)	3603.2(16)	21.6(5)
C6	5482(2)	4602(3)	4193.9(15)	17.8(5)
C7	7232(2)	4413(3)	5134.4(15)	18.2(5)
C8	8367(2)	4735(3)	5748.1(15)	18.4(5)
C9	9128(2)	5680(3)	5614.1(17)	25.2(6)
C10	10147(3)	5942(3)	6254.9(19)	31.4(7)
C11	10367(3)	5249(3)	6991.1(17)	27.9(6)
C12	9575(2)	4279(3)	7053.3(17)	24.0(6)
C13	6654(2)	6789(3)	4524.1(16)	18.5(5)
C14	7165(2)	7130(3)	3848.8(15)	17.9(5)
C15	6775(3)	6491(3)	3077.6(17)	21.0(6)
C16	7239(2)	6841(3)	2463.5(17)	23.7(6)
C17	8094(2)	7825(3)	2637.1(17)	22.8(6)
C18	8507(3)	8470(3)	3387.1(18)	24.4(6)
C19	8027(2)	8116(3)	3996.5(16)	21.5(5)

Table 2: Anisotropic Displacement Parameters (×10⁴) **2018ncs0303**. The anisotropic displacement factor exponent takes the form: $-2\pi^2[h^2a^{*2} \times U_{11} + \ldots + 2hka^* \times b^* \times U_{12}]$

Atom	U_{11}	U_{22}	U_{33}	U_{23}	U_{13}	U_{12}
Au1	19.58(7)	16.47(7)	14.74(7)	1.17(3)	4.82(5)	-2.22(4)
Cl1	25.3(3)	25.6(3)	22.6(3)	1.9(2)	11.6(3)	-0.7(2)
Cl2	28.3(3)	20.5(3)	24.7(3)	4.7(2)	9.0(3)	2.0(2)
Cl3	23.8(3)	22.8(3)	22.0(3)	4.2(2)	9.7(3)	-1.5(2)
F1	44.0(10)	32.2(9)	30.9(9)	6.7(7)	24.7(8)	1.2(8)
N1	19.2(11)	17.7(10)	15.9(10)	0.8(9)	4.8(8)	-3.3(9)
N2	18.7(10)	16.9(10)	14.8(10)	1.6(8)	5.2(8)	-1.8(8)
N3	21.7(11)	20.3(11)	18.6(11)	2.1(9)	5.1(9)	-1.3(9)
C1	19.4(13)	22.7(12)	13.2(12)	-2.3(10)	6.4(10)	-2.0(10)
C2	24.6(13)	25.8(14)	18.2(12)	-1.9(11)	10.0(11)	-5.4(11)
C3	22.0(13)	31.4(15)	18.5(13)	-5.8(11)	8.7(11)	-10.0(11)
C4	18.5(13)	35.6(16)	16.6(12)	-3.4(11)	4.8(10)	0.9(12)
C5	22.9(13)	25.7(14)	17.9(12)	1.0(10)	9.1(10)	1.4(11)
C6	19.4(12)	22.6(13)	12.7(11)	-3.0(10)	7.1(10)	-4.2(10)
C7	19.7(12)	21.2(13)	14.5(11)	1.5(10)	6.6(10)	-1.0(10)
C8	19.7(12)	17.1(12)	17.4(12)	0.7(10)	4.6(10)	-1.1(10)
C9	23.7(14)	29.0(15)	20.5(13)	7.3(11)	3.7(11)	-4.6(11)
C10	28.1(15)	31.6(16)	30.0(15)	8.4(13)	3.1(12)	-10.5(13)
C11	26.1(14)	29.7(15)	22.7(14)	2.0(11)	0.6(11)	-4.2(12)
C12	26.0(14)	26.2(14)	18.1(13)	3.8(11)	4.9(11)	0.6(11)
C13	23.6(13)	15.4(12)	16.8(12)	-0.3(10)	7.1(10)	-1.7(10)
C14	21.3(12)	15.7(12)	17.1(12)	3.8(9)	6.9(10)	2.2(10)
C15	26.1(14)	18.1(14)	19.2(14)	1.2(9)	8.1(12)	-0.3(10)
C16	34.0(16)	20.1(13)	17.9(13)	1.0(11)	9.6(11)	2.8(12)
C17	28.8(14)	21.9(13)	22.9(13)	8.1(11)	15.4(11)	5.9(11)
C18	22.8(14)	21.6(14)	28.1(15)	7.5(10)	7.3(12)	-0.8(10)
C19	24.8(14)	20.0(13)	18.6(13)	1.9(10)	5.4(11)	0.6(11)

Table 3: Bond Lengths in Å for **2018ncs0303**.

Atom	Atom	Length/Å
Au1	Cl1	2.2802(6)
Au1	Cl2	2.2718(6)
Au1	Cl3	2.2902(6)
Au1	N1	2.024(2)
F1	C17	1.358(3)
N1	C1	1.393(3)
N1	C7	1.337(3)
N2	C6	1.393(3)
N2	C7	1.355(3)
N2	C13	1.479(3)
N3	C8	1.347(3)
N3	C12	1.330(4)
C1	C2	1.388(4)
C1	C6	1.401(4)
C2	C3	1.383(4)
C3	C4	1.400(4)
C4	C5	1.387(4)
C5	C6	1.388(4)
C7	C8	1.474(4)
C8	C9	1.380(4)
C9	C10	1.388(4)
C10	C11	1.376(4)
C11	C12	1.383(4)
C13	C14	1.516(3)
C14	C15	1.395(4)
C14	C19	1.387(4)
C15	C16	1.387(4)
C16	C17	1.379(4)
C17	C18	1.369(4)
C18	C19	1.394(4)

Table 4: Bond Angles in ° for **2018ncs0303**.

Atom	Atom	Atom	Angle/°
Cl1	Au1	Cl3	176.75(2)
Cl2	Au1	Cl1	89.13(2)
Cl2	Au1	Cl3	91.36(2)
N1	Au1	Cl1	89.39(6)
N1	Au1	Cl2	178.43(6)
N1	Au1	Cl3	90.09(6)
C1	N1	Au1	126.63(18)
C7	N1	Au1	125.13(17)
C7	N1	C1	108.0(2)
C6	N2	C13	123.6(2)
C7	N2	C6	108.1(2)
C7	N2	C13	128.2(2)
C12	N3	C8	117.0(2)
N1	C1	C6	107.3(2)
C2	C1	N1	131.1(3)
C2	C1	C6	121.6(2)
C3	C2	C1	116.5(3)
C2	C3	C4	121.8(2)
C5	C4	C3	122.0(2)
C4	C5	C6	116.0(3)
N2	C6	C1	106.4(2)
C5	C6	N2	131.6(2)
C5	C6	C1	122.1(2)
N1	C7	N2	110.2(2)
N1	C7	C8	122.9(2)
N2	C7	C8	126.8(2)
N3	C8	C7	113.1(2)
N3	C8	C9	123.4(2)
C9	C8	C7	123.5(2)
C8	C9	C10	118.1(2)
C11	C10	C9	119.3(3)
C10	C11	C12	118.3(3)
N3	C12	C11	123.8(3)
N2	C13	C14	113.4(2)
C15	C14	C13	121.5(2)
C19	C14	C13	119.3(2)
C19	C14	C15	119.3(2)
C16	C15	C14	120.4(3)
C17	C16	C15	118.4(3)
F1	C17	C16	117.9(2)
F1	C17	C18	119.0(3)
C18	C17	C16	123.0(2)
C17	C18	C19	118.0(3)
C14	C19	C18	120.9(3)

Table 5: Torsion Angles in ° for **2018ncs0303**.

Atom	Atom	Atom	Atom	Angle/°
Au1	N1	C1	C2	3.6(4)
Au1	N1	C1	C6	-175.69(16)
Au1	N1	C7	N2	174.79(16)
Au1	N1	C7	C8	-9.0(3)
F1	C17	C18	C19	-179.6(2)
N1	C1	C2	C3	-179.7(3)
N1	C1	C6	N2	1.3(3)
N1	C1	C6	C5	-179.7(2)
N1	C7	C8	N3	-32.8(3)
N1	C7	C8	C9	146.9(3)
N2	C7	C8	N3	142.7(3)
N2	C7	C8	C9	-37.5(4)
N2	C13	C14	C15	44.0(3)
N2	C13	C14	C19	-137.0(2)
N3	C8	C9	C10	-3.4(4)
C1	N1	C7	N2	-0.4(3)
C1	N1	C7	C8	175.8(2)
C1	C2	C3	C4	-0.2(4)
C2	C1	C6	N2	-178.0(2)
C2	C1	C6	C5	1.0(4)
C2	C3	C4	C5	0.4(4)
C3	C4	C5	C6	0.1(4)
C4	C5	C6	N2	178.0(2)
C4	C5	C6	C1	-0.7(4)
C6	N2	C7	N1	1.3(3)
C6	N2	C7	C8	-174.8(2)
C6	N2	C13	C14	-90.7(3)
C6	C1	C2	C3	-0.5(4)
C7	N1	C1	C2	178.7(3)
C7	N1	C1	C6	-0.6(3)
C7	N2	C6	C1	-1.6(3)
C7	N2	C6	C5	179.6(3)
C7	N2	C13	C14	93.4(3)
C7	C8	C9	C10	176.9(3)
C8	N3	C12	C11	-0.1(4)
C8	C9	C10	C11	0.6(5)
C9	C10	C11	C12	2.1(5)
C10	C11	C12	N3	-2.4(5)
C12	N3	C8	C7	-177.2(2)
C12	N3	C8	C9	3.1(4)
C13	N2	C6	C1	-178.2(2)
C13	N2	C6	C5	3.0(4)
C13	N2	C7	N1	177.7(2)
C13	N2	C7	C8	1.6(4)
C13	C14	C15	C16	178.6(2)
C13	C14	C19	C18	-179.1(2)
C14	C15	C16	C17	0.4(4)
C15	C14	C19	C18	-0.2(4)
C15	C16	C17	F1	179.1(2)
C15	C16	C17	C18	0.0(4)
C16	C17	C18	C19	-0.5(4)
C17	C18	C19	C14	0.6(4)
C19	C14	C15	C16	-0.3(4)

Table 6: Hydrogen Fractional Atomic Coordinates ($\times 10^4$) and Equivalent Isotropic Displacement Parameters ($Å^2 \times 10^3$) for **2018ncs0303**. U_{eq} is defined as 1/3 of the trace of the orthogonalised U_{ij}.

Atom	x	y	z	U_{eq}
H2	4941	1321	4327	27
H3	3215	2012	3320	28
H4	2917	4272	2884	29
H5	4339	5953	3424	26
H9	8959	6138	5098	30
H10	10687	6593	6186	38
H11	11047	5432	7445	34
H12	9744	3777	7555	29
H13A	7170	7156	5056	22
H13B	5894	7250	4399	22
H15	6189	5811	2972	25
H16	6973	6414	1936	28
H18	9102	9139	3489	29
H19	8293	8555	4520	26

Citations

CrysAlisPro Software System, Rigaku Oxford Diffraction, (2018).

O.V. Dolomanov and L.J. Bourhis and R.J. Gildea and J.A.K. Howard and H. Puschmann, Olex2: A complete structure solution, refinement and analysis program, *J. Appl. Cryst.*, (2009), **42**, 339-341.

Sheldrick, G.M., Crystal structure refinement with ShelXL, *Acta Cryst.*, (2015), **C27**, 3-8.

Sheldrick, G.M., ShelXT-Integrated space-group and crystal-structure determination, *Acta Cryst.*, (2015), **A71**, 3-8.

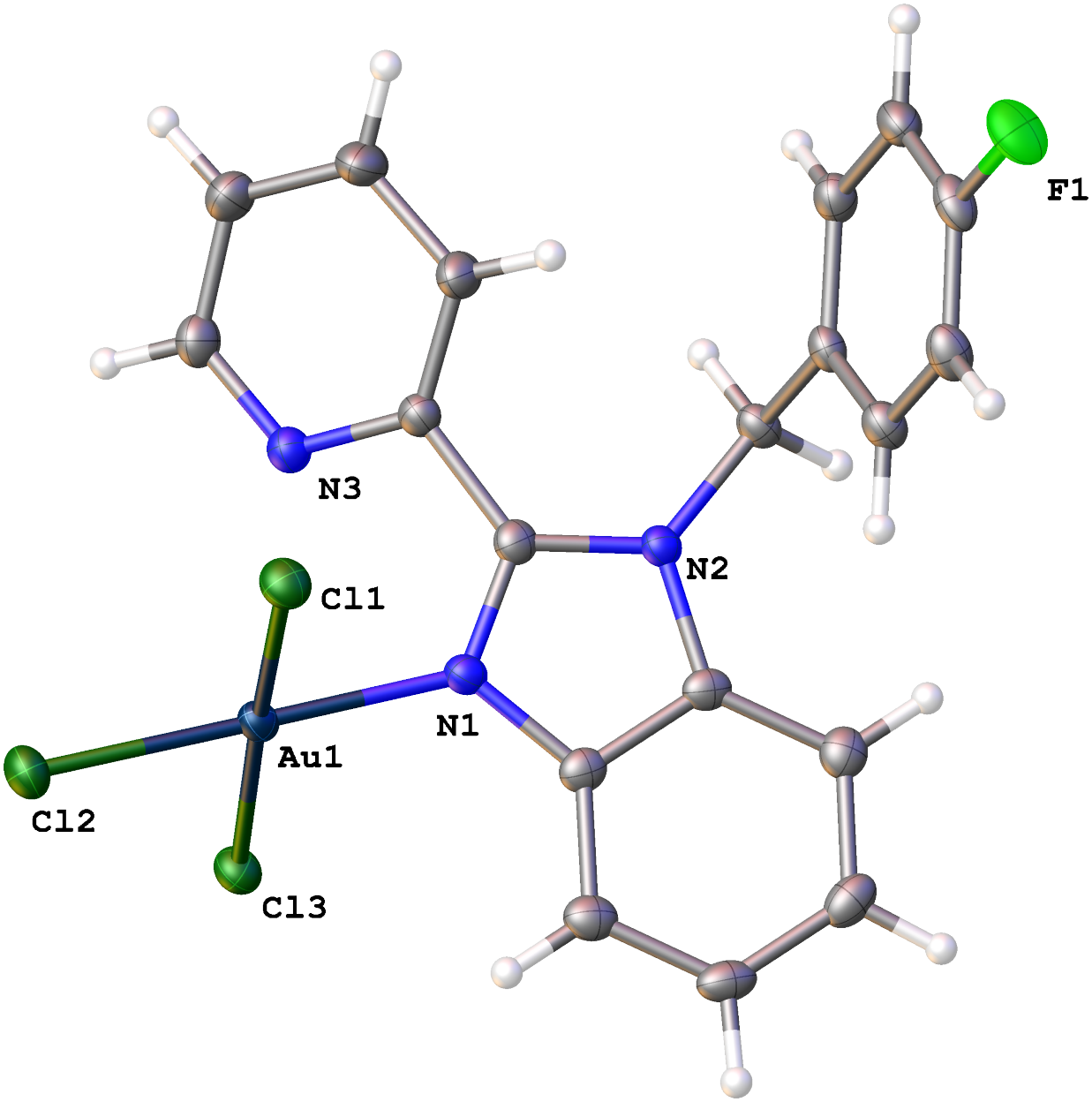
F1
N3
N2
Cl1
N1
Au1
Cl2
Cl3